NOAA Technical Memorandum ERL PMEL-92

THE ANNUAL MEAN TRANSPORT IN PUGET SOUND

E. D. Cokelet
R. J. Stewart
C. C. Ebbesmeyer

Pacific Marine Environmental Laboratory
Seattle, Washington
July 1990

noaa NATIONAL OCEANIC AND ATMOSPHERIC ADMINISTRATION / Environmental Research Laboratories

NOAA Technical Memorandum ERL PMEL-92

THE ANNUAL MEAN TRANSPORT IN PUGET SOUND

E. D. Cokelet
Pacific Marine Environmental Laboratory

R. J. Stewart
The Digital Analogics Company
Seattle, Washington

C. C. Ebbesmeyer
Evans-Hamilton, Inc.
Seattle, Washington

Pacific Marine Environmental Laboratory
Seattle, Washington
July 1990

UNITED STATES DEPARTMENT OF COMMERCE

Robert A. Mosbacher
Secretary

NATIONAL OCEANIC AND ATMOSPHERIC ADMINISTRATION

John A. Knauss
Under Secretary for Oceans and Atmosphere/Administrator

Environmental Research Laboratories

Joseph O. Fletcher
Director

NOTICE

Mention of a commercial company or product does not constitute an endorsement by NOAA/ERL. Use of information from this publication concerning proprietary products or the tests of such products for publicity or advertising purposes is not authorized.

Contribution No. 1201 from NOAA/Pacific Marine Environmental Laboratory

For sale by the National Technical Information Service, 5285 Port Royal Road
Springfield, VA 22161

CONTENTS

Page

List of Figures iv

List of Tables v

ABSTRACT 1

1. INTRODUCTION 1

2. THEORY AND APPROXIMATIONS 5

2.1 Knudsen's Relations 5
2.2 Representativeness of Midchannel Observations 9
2.3 Time Averaging 10
2.4 Error Analysis 12

3. REACHES AND MIXING ZONES 15

4. RUNOFF 18

5. CURRENTS 24

6. SALINITY 31

7. TRANSPORT 36

7.1 Strait of Juan de Fuca 40
7.2 Puget Sound's Main Axis 40
7.3 Hood Canal 43
7.4 Saratoga Passage and Deception Pass 43
7.5 Comparison with other models 46
7.6 Knudsen Transport Terms 47
7.7 Error Contributions 47

8. SUMMARY AND CONCLUSIONS 49

9. ACKNOWLEDGMENTS 50

10. REFERENCES 50

11. APPENDIX 55

FIGURES

Page

Figure 1a. Map of the Strait of Juan de Fuca 2

Figure 1b. Map of Puget Sound 3

Figure 2. Along-channel section of the Strait of Juan de Fuca/Puget Sound system 4

Figure 3. A schematic view of a fjord 7

Figure 4. The channel cross sections as seen looking seaward 11

Figure 5. The Puget Sound watersheds 19

Figure 6. The annual mean runoff R_i entering each mixing zone of the Strait of Juan de Fuca and Puget Sound 23

Figure 7. The annual mean cumulative runoff $R_{i\Sigma}$ entering the Strait of Juan de Fuca and Puget Sound landward of each reach 26

Figure 8. Composite vertical profiles of the velocity normal to each reach cross section 29

Figure 9. Vertical profiles of the mean and flux-weighted salinities for each reach layer as numbered 32

Figure 10. Time series of the annual mean flux-weighted salinity S_i for each reach layer 34

Figure 11. Time series of the annual mean landward transports $Q_{2j-1}/\overline{\rho}$ in each reach 39

Figure 12. Schematic diagram of the Deception Pass region 44

TABLES

Page

Table 1. The cross-sectional areas A_i of the reach layers 16

Table 2. Coefficients for calculating the runoff into the Puget Sound basins from USGS gauging stations (adapted from Lincoln, 1977) 21

Table 3. Portions of the watershed runoff entering the mixing zones and their May 1951–December 1955 mean and standard deviation 22

Table 4. Correlations between the annual mean runoff R_i 25

Table 5. The overall mean mixing zone runoff R_i, cumulative runoff $R_{i\Sigma}$ and their standard deviations 25

Table 6. Sources and years of current observations and average directions of cross section unit normal vector $\underset{\sim}{n}$ 27

Table 7. Inventory of current meter records and hydrographic casts 28

Table 8. Bottom depth D, regression equation and zero-crossing depth z_0 for the normal velocity $\bar{u} \cdot n$ as a function of depth z (m), squared correlation coefficient r^2 and the standard error of the regression 30

Table 9. Correlations between the flux-weighted salinities 35

Table 10. Correlations between the flux-weighted salinities and the runoff 37

Table 11. Average percentage contribution to the within-year variance $\overline{\Delta S_i^2}$ in the flux-weighted salinities 37

Table 12. The overall mean flux-weighted salinities and transports with their standard deviations 38

Table 13. Comparison of the volume transports (m^3/s) range from Knudsen's equations with composite transports and previous estimates 41

Table 14. Correlations between the landward transport Q_{2j-1} in each reach and the terms in Knudsen's equations (7) 48

Table 15. Average percentage contribution to the within-year variance in the transports 48

The Annual Mean Transport in Puget Sound

E.D. Cokelet[1], R.J. Stewart[2], and C.C. Ebbesmeyer[3]

ABSTRACT. Puget Sound is modeled as a branched system of two-layered advective reaches separated by mixing zones. Fresh water and salt provide convenient tracers to calculate the annual mean layer transports. The technique utilizes historical records (1951–1956) of runoff and salinity which are analyzed with the aid of modern (principally 1970's) current meter records to provide the appropriate mass conserving landward- and seaward-flowing layer salinities for each reach. This is the first time that the long-term transports have been estimated simultaneously for the entire Strait of Juan de Fuca/Puget Sound system. With few exceptions the inferred transports agree well with estimates derived from scattered, shorter duration current observations. Uncertainties in the transports are estimated from uncertainties in the runoff, velocity profiles and salinities. The results provide the basis for future computations of refluxing and the steady state tracer concentrations and ages in the Sound.

1. INTRODUCTION

Puget Sound is a glacially carved fjordlike estuary located in the northwestern United States and connected to the Pacific Ocean via the Strait of Juan de Fuca (Figure 1). By the year 2000 the population of its watershed is projected to increase by 20% to 3.6 million people (Washington Office of Financial Management, 1987). With this increasing urbanization the long-term circulation of the Sound and its relationship to the transport and dispersal of pollutants are becoming of increasing concern. Since in a fjord the normal mean circulation pattern is seaward flow at the surface and compensating landward flow at depth (Hansen and Rattray, 1966) one might expect that contaminants introduced to the surface layers of Puget Sound would be carried out to sea. However, the Sound is composed of a series of deep reaches separated by usually shallower mixing zones where rivers enter and tidal currents accelerate (Figures 1 and 2). Ebbesmeyer and Barnes (1980) estimated that within mixing zone 2 seaward of the major cities, about 2/3 of the seaward flow would recirculate or reflux landward due to vertical advection and mixing. This could have a profound effect on pollutant concentrations in Puget Sound. They did not consider refluxing within other Puget Sound mixing zones.

Ebbesmeyer, Coomes, Cannon and Bretschneider (1989) have recently detected climatic signals in the Pacific Northwest and Puget Sound. As the winter Aleutian Low shifts position from west to east, Northwest weather oscillates between relatively cool, wet and warm, dry conditions. Each cycle takes 15 to 20 years on average. Evidence from a partial cycle suggests that the landward flow in reach 3 of Puget Sound (Figure 2) fluctuates between periods of mid-depth and bottom intensification in response to an alternately reduced and enhanced horizontal salinity gradient across Admiralty Inlet sill in mixing zone 2. Data are insufficient to show

[1] Pacific Marine Environmental Laboratory/NOAA, 7600 Sand Point Way NE, Seattle, WA 98115–0070
[2] 4116 55th Ave. SW, Seattle, WA 98116
[3] Evans-Hamilton, Inc., 731 N. Northlake Way, Suite 201, Seattle, WA 98103

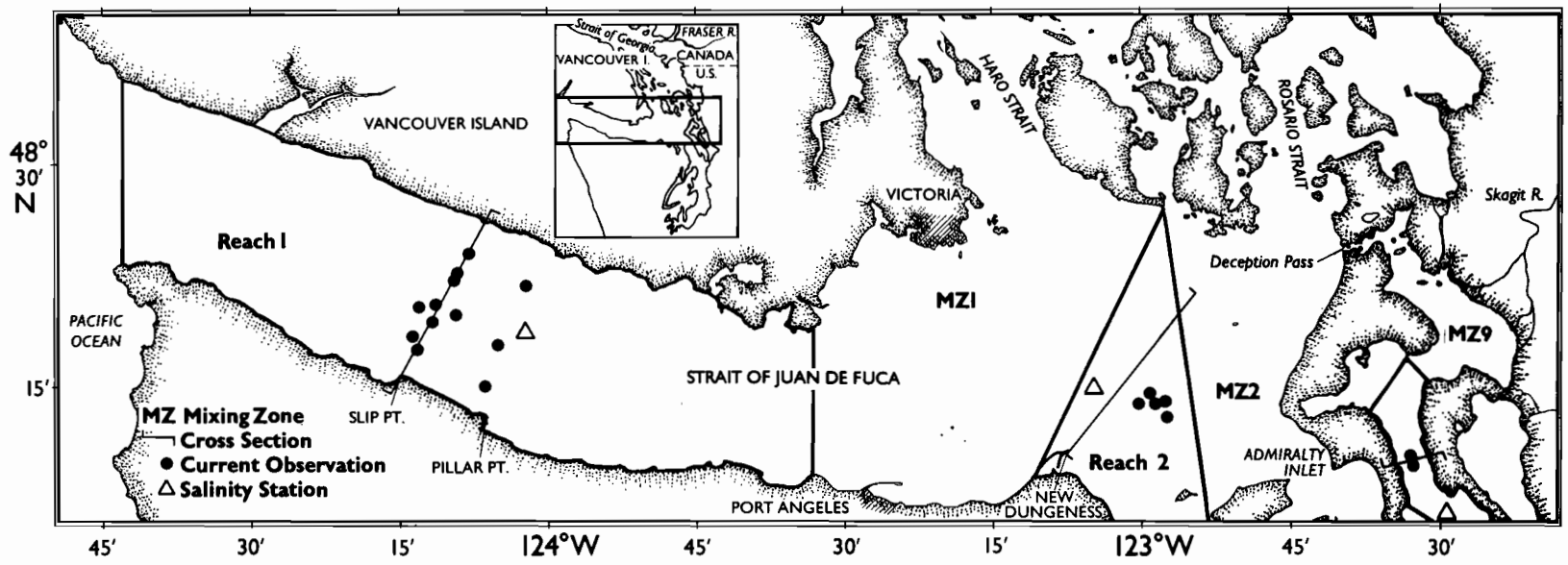

Figure 1a. Map of the Strait of Juan de Fuca showing the reaches (outlined), mixing zones (MZ) and sites of channel cross sections, current observations and salinity stations. The inset shows the Strait of Georgia and the Fraser River.

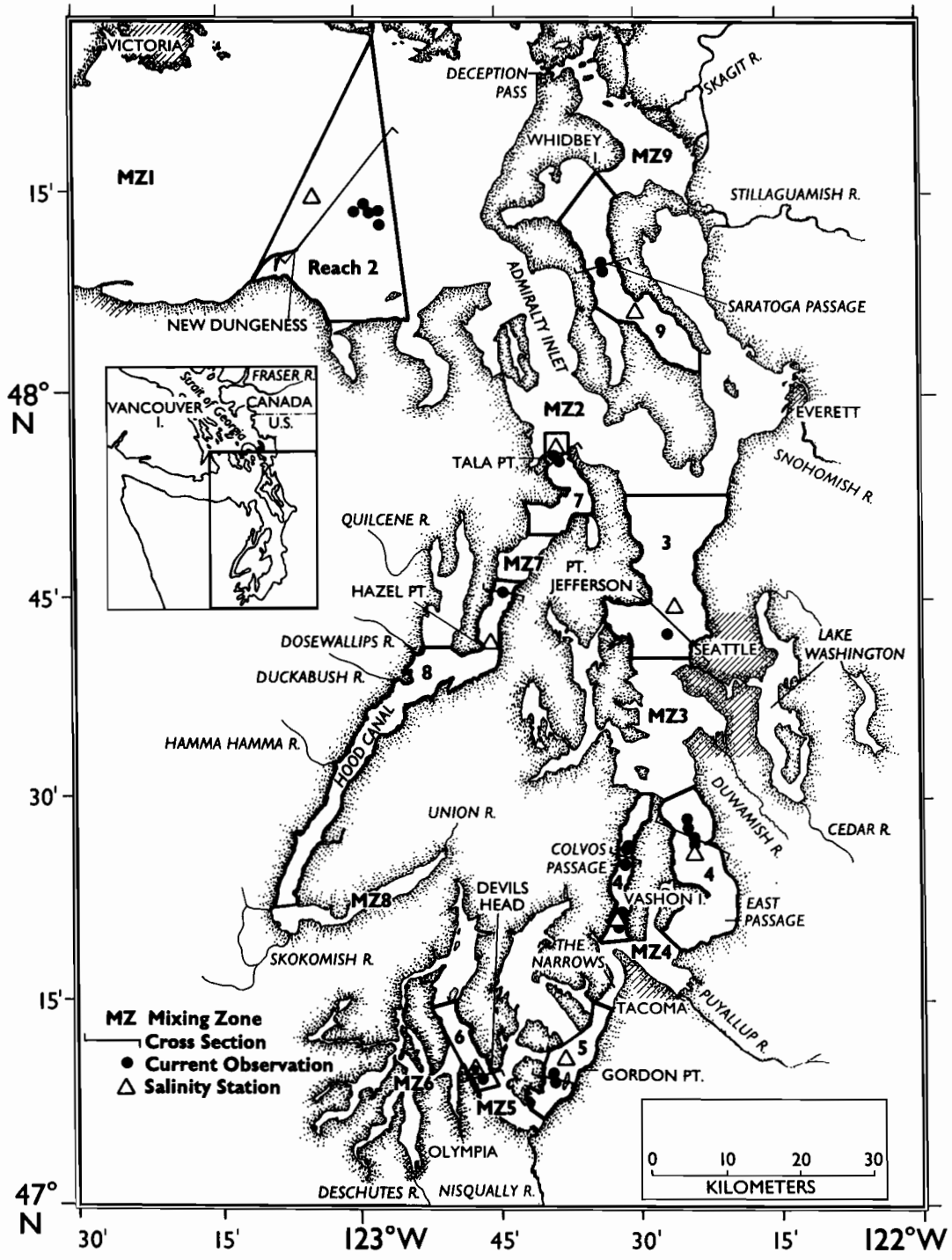

Figure 1b. Map of Puget Sound showing the reaches (outlined), mixing zones (MZ) and sites of channel cross sections, current observations and salinity stations.

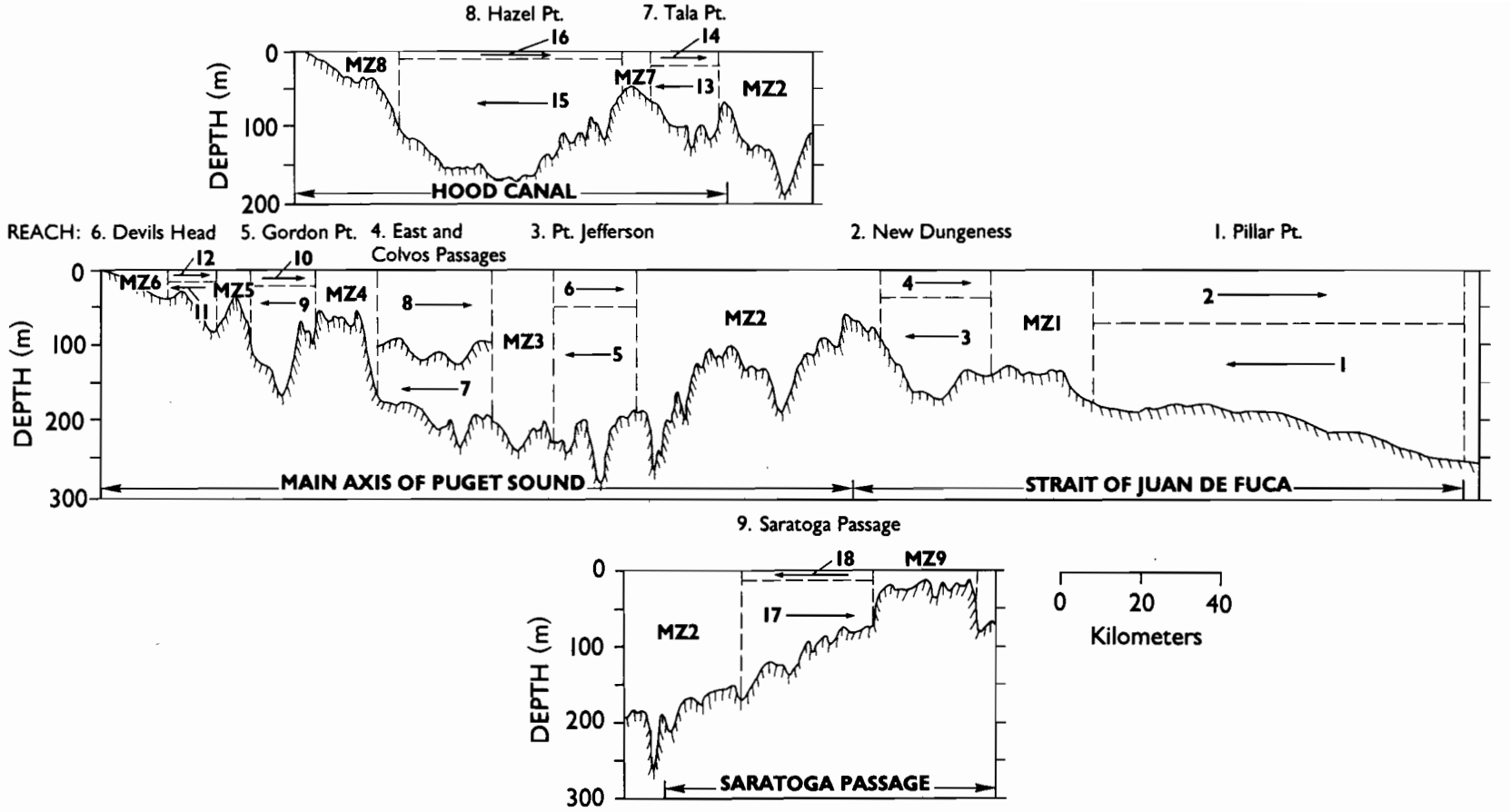

Figure 2. Along-channel section of the Strait of Juan de Fuca/Puget Sound system. The reach layers are numbered such that landward-flowing layers are odd, and seaward-flowing layers are even. The four principal geographic regions—the Strait of Juan de Fuca, the main axis of Puget Sound, Hood Canal and Saratoga Passage—are labeled. (Bottom profile adapted from Collias *et al.*, 1974.)

whether other Puget Sound reaches respond similarly. What effect climatic oscillations have on the strength of the two-layer circulation remains unknown.

Hydrographic observations in Puget Sound date back to 1930 (Collias and Andreeva, 1972) with the period 1951 to 1956 being the most intensively sampled. During that time several water bottle stations covering the major portions of the Strait of Juan de Fuca and Puget Sound were resampled at approximately six-week intervals (Collias, 1970). This effort has never been equalled nor is it likely to be in the foreseeable future. Although extensive in space and time, this data set has never been fully and systematically utilized to infer the transport in Puget Sound. During the 1970's and 1980's research priorities turned to moored current observations of a few weeks-to-months duration at selected sites mostly in midchannel (Cannon, 1983; Cox *et al.*, 1984). The currents in the major reaches have been measured, but never simultaneously.

The problems of pollutant build-up and climatic change are long-term and require long-term observations and models to address them. Cokelet and Stewart (1985) laid out a technique for calculating the transport, refluxing, and pollutant concentrations and ages in fjords using runoff and salinity observations. The purpose of this report is to take the first step in Puget Sound, namely, to calculate systematically the annual mean runoff, salinity and transport. We shall use the extensive data set of the 1950's, a period of cool, wet conditions (Ebbesmeyer *et al.*, 1989) and thereby produce the first complete estimate of transport in this climatic regime.

This report is arranged in 8 sections and an appendix. In Section 2 we review the theory and approximations involved in the analysis. One new contribution is an error analysis in which uncertainties in the transports are related to fluctuations in the runoff, currents and salinities. Section 3 enumerates the nine major reaches and mixing zones of the Strait of Juan de Fuca/Puget Sound system. The annual mean runoff entering each mixing zone is computed in Section 4. Composite vertical current profiles are constructed from short-term velocity measurements in each reach (Section 5). These are used in conjunction with the salinity observations to produce time series of the flux-weighted salinity in each reach layer (Section 6). Volume transports are computed and compared with previous estimates (Section 7). Section 8 contains the summary and conclusions. Details of the time series analysis and error estimates are given in the Appendix.

2. THEORY AND APPROXIMATIONS

2.1 Knudsen's Relations

The mean two-layered flow in an estuary can be deduced by applying the principle of mass conservation to water and salt. The mean advective transport Q_i of total mass (water + salt) in layer i is the integral over the layer cross-sectional area A_i of the product of the fluid density ρ and the normal component of velocity $\underset{\sim}{u} \cdot \underset{\sim}{n}$, i.e.

$$Q_i = (-1)^i \int_{A_i} \overline{\rho}\ \overline{\underset{\sim}{u}} \cdot \underset{\sim}{n}\ dA \tag{1}$$

where $\underset{\sim}{n}$ is a seaward-pointing unit normal vector (Cokelet and Stewart, 1985, henceforth referred to as I). An overbar represents a time average over a sufficient period (one year, say) that the estuary's volume and salinity are steady. Odd-indexed layers i = 2j–1, j = 1,2,..., flow landward, and even-indexed layers i = 2j flow seaward (Figure 3). Applying (1) to an estuarine cross-section in which the cumulative runoff entering landward of reach j is $R_{j\Sigma}$ yields

$$Q_{2j-1} + R_{j\Sigma} = Q_{2j}. \tag{2}$$

This means that the mass of water entering and leaving the estuarine segment balance. Similarly salt conservation gives

$$S_{2j-1}\ Q_{2j-1} + F_{2j-1} + F_{2j} = S_{2j}\ Q_{2j} \tag{3}$$

where S_i, i = 2j–1, 2j, is the mean flux-weighted salinity in layer i defined by

$$S_i = \frac{(-1)^i}{Q_i} \int_{A_i} \overline{\rho}\ \overline{S}\ \overline{\underset{\sim}{u}} \cdot \underset{\sim}{n}\ dA. \tag{4}$$

F_i is the turbulent transport of salt through A_i given by

$$F_i = -\overline{\rho} \int_{A_i} \overline{S'\underset{\sim}{u}'} \cdot \underset{\sim}{n}\ dA. \tag{5}$$

The quantities $\underset{\sim}{u}'$ and S′ are the fluctuations of the velocities and salinities about their mean values. Equation (3) means that the seaward, advective flux of salt in layer 2j, $S_{2j}\ Q_{2j}$, equals the landward, advective flux plus the landward turbulent flux in both layers. Turbulence here means fluctuations over a time scale less than the averaging period. Combining (2) and (3) yields

$$\begin{aligned} Q_{2j-1} &= \frac{S_{2j}\ R_{j\Sigma} - (F_{2j-1} + F_{2j})}{S_{2j-1} - S_{2j}} \\ Q_{2j} &= \frac{S_{2j-1}\ R_{j\Sigma} - (F_{2j-1} + F_{2j})}{S_{2j-1} - S_{2j}} \end{aligned} \tag{6}$$

for the layer transports. In layers where the turbulent transports are negligible equations (6) reduce to Knudsen's (1900) equations

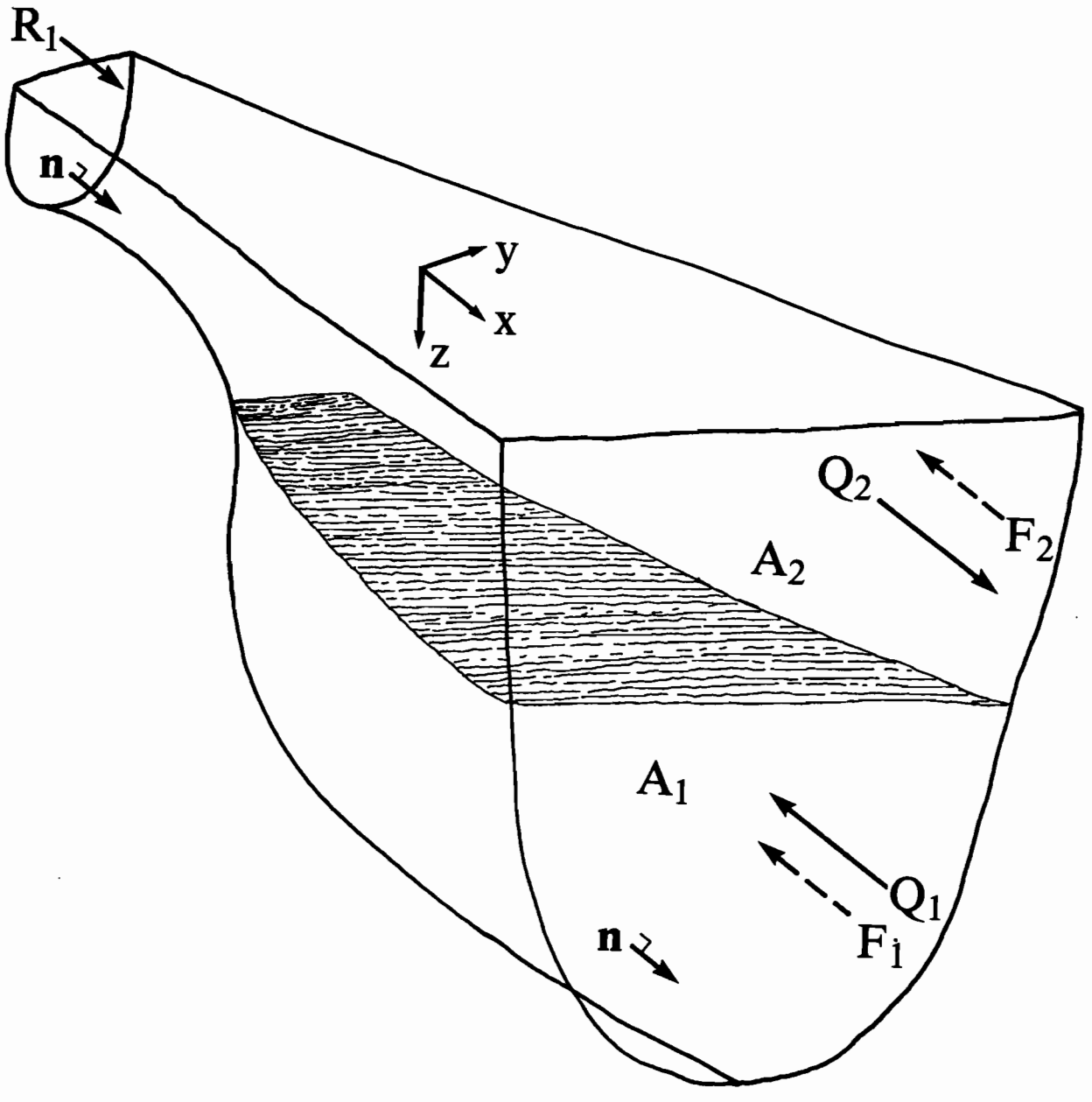

Figure 3. A schematic view of a fjord showing the advective flux Q_i of seawater moving through cross-sections A_i with seaward-pointing unit normal vector $\underset{\sim}{n}$. Runoff R_1 enters through the river at the fjord's head. Salt is transported by advective S_iQ_i and turbulent F_i fluxes (positive in the direction of the arrows). (Adapted from Cokelet and Stewart (1985).)

$$Q_{2j-1} = \frac{S_{2j}}{S_{2j-1} - S_{2j}} R_{j\Sigma}$$

$$Q_{2j} = \frac{S_{2j-1}}{S_{2j-1} - S_{2j}} R_{j\Sigma} \tag{7}$$

which relate the mean advective transports to the flux-weighted salinities and the runoff.

The reaches to be described in Section 3 are sited where the turbulent salt flux terms can be neglected. From (6) this requires

$$F_i << S_i R_{j\Sigma} \qquad i = 2j\text{–}1, 2j. \tag{8}$$

The turbulent salt flux can be related to the mean longitudinal salinity gradient $\frac{d\bar{S}}{dx}$ (Dyer, 1973) by

$$F_i = \bar{\rho} \int_{A_i} K \frac{d\bar{S}_i}{dx} dA$$

$$\approx \bar{\rho} K \frac{d\bar{S}_i}{dx} A_i \tag{9}$$

where K is the eddy diffusivity. Appropriate values for Puget Sound are K ~ 10^6 cm^2/s (Okubo, 1971; Officer, 1977), $\frac{dS}{dx}$ ~ 0.02 ‰/km, A ~ 0.25 km^2, S ~ 30 ‰, R/ρ ~ 200 m^3/s. Equation (8) becomes

$$F_i \sim 500 \text{ kg/s} << S_i R_{j\Sigma} \sim 6000 \text{ kg/s}. \tag{10}$$

This agrees with Hansen and Rattray's (1966) classification of the Strait of Juan de Fuca as a Type 3 estuary in which the diffusive salt flux is less than 1% of the advective salt flux.

Ideally, simultaneous, long-term current observations at several sites spanning a reach channel are sufficient to calculate Q_i from (1) directly. Unfortunately the number of current observations available in Puget Sound (and in most estuaries) is far from ideal. They are asynchronous, short-duration, scattered observations usually taken at midchannel, and none cover the 1951 to 1956 period. Even if they did, to use them alone would run the risk of calculating transports that are inconsistent with mass conservation. To make valid predictions from the reflux theory (I) we require two-layer salinities and transports that together conserve mass. These are obtained from Knudsen's equations (7) in which fresh water and salt act as tracers. Of course these constituents have dynamical significance, but this is inaccessible in a pure mass-conservation formulation. Some dynamical factors such as the sea-surface and internal-interface slopes were not measured or poorly resolved in the 1950's data set; therefore a complete dynamical analysis cannot be performed. However, nature did provide us with a grand experiment—the freshening of the salty brine—from which we can learn much.

At first glance Knudsen's equations (7) seem to provide a way to compute transports from salinities and runoff alone without the need for velocity observations, but (4) shows that

velocities are required to calculate the flux-weighted salinities S_i. In previous applications of Knudsen's equations it has been implicitly assumed that the velocity effect approximately cancels in (4) due to the Q_i term in the denominator; therefore the integration involves only salinity and density over the cross section. However, this approach suffers from the fact that the position of the interface between landward- and seaward-flowing layers is unknown. It is usually placed at the level of maximum vertical salinity gradient, the halocline, but this does not necessarily coincide with the level of vanishing mean velocity, the level-of-no-net-motion.

We adopt a different approach. As mentioned previously, no simultaneous current measurements were taken during the period of study, but sufficient current data do exist to construct composite velocity profiles for each major reach from a statistical fit to the scattered, short-term observations. These offer several advantages over neglecting the velocity effects altogether. They provide:

(1) the direction of the cross-section normal vector,

(2) the level-of-no-net-motion, and

(3) the flux-weighting functions $\overline{\underset{\sim}{u}} \cdot \underset{\sim}{n}$.

Fortuitously the currents were mostly measured during the 1970's in the next cool, wet climatic cycle following that of the 1950's (Ebbesmeyer *et al.*, 1989). Therefore if the current profiles do change with the climatic regime as suggested for reach 3 then we have consistent, but not concurrent, salinities and velocities.

2.2 Representativeness of Midchannel Observations

All of the salinities and the majority of the currents were measured at midchannel sites (Figure 1). Therefore the cross-sectional area integrals of (4) are approximated by

$$S_i \approx \frac{\int \overline{S} \int \overline{\underset{\sim}{u}} \cdot \underset{\sim}{n} \, dy \, dz}{\iint \overline{\underset{\sim}{u}} \cdot \underset{\sim}{n} \, dy \, dz} \approx \frac{\int_{z_1}^{z_2} \overline{S} \, \overline{\underset{\sim}{u}} \cdot \underset{\sim}{n} \, w \, dz}{\int_{z_1}^{z_2} \overline{\underset{\sim}{u}} \cdot \underset{\sim}{n} \, w \, dz} \tag{11}$$

where w(z) is the channel width, and z_1 and z_2 are the upper and lower depths of each layer. The mean density variation with depth is negligible; hence $\overline{\rho}$ has been taken outside the integrals. Since the effects of the earth's rotation complicate the cross-channel current structure, a midchannel approximation is valid in a strict sense only if the channel width is less than the internal Rossby radius of deformation

$$a = \frac{N}{mf} \approx \frac{\sqrt{g'h}}{f} \tag{12}$$

where N is the Brünt-Väisälä frequency, m is the vertical wave number, f is the Coriolis parameter, $g' = \frac{\Delta\rho}{\rho} g$ is the reduced gravitational acceleration, $\Delta\rho$ is a typical vertical density difference, and h is the water depth (Gill, 1982). For reach 1 in the western Strait of Juan de Fuca the Rossby radius is about 10 km for vertical mode number 1 internal waves which dominate the transient response to nonlocal wind forcing with periods of a few days (Proehl and Rattray, 1984). The channel width (20 km, Figure 4) exceeds this value, hence the cross-channel current structure ought to be included. Observations indicate that the salinity field varies much less across channel (Cannon and Bretschneider, 1986), and midchannel salinity values are representative. In the eastern Strait and Puget Sound $\Delta\rho/\rho \sim 10^{-3}$, h ~ 200 m, and the Rossby radii for mode numbers 1 and 2 waves are about 14 and 7 km, respectively. The widths of reaches 2 and 3 fall into this range (Figure 4), but only midchannel current observations exist there (Figure 1). However, observations in the more transient western Strait show that currents averaged over a month or longer are much more uniform across channel than daily averaged currents (Cannon and Bretschneider, 1986). Therefore in the eastern Strait and Puget Sound we will proceed with record-averaged midchannel currents usually of one-to-several-months duration.

2.3 Time Averaging

The runoff and salinities are averaged over a period of one year using a time-centered moving average defined by

$$\bar{f}(\underset{\sim}{x}) \equiv \frac{1}{T} \int_{t-\frac{T}{2}}^{t+\frac{T}{2}} f(\underset{\sim}{x},t')dt'. \tag{13}$$

This is a minor departure from the time-advanced mean of I, and it has no effect on the theoretical derivations.

One way to estimate the annual mean for monthly sampled data, say, would be to compute the arithmetic mean and variance s^2 from N = 12 consecutive data points. The standard error defined by $s/N^{1/2}$ is a measure of the uncertainty in the mean. However, this would lead to a pessimistic estimate with the quasi-periodic annual signal contributing substantially to the error. A better way to proceed is to recognize that the time series consists of a systematic part—the mean plus the quasi-periodic annual component—and a stochastic part—the noise. Estimating the noise will provide a better measure of the mean's uncertainty. To achieve this we estimate

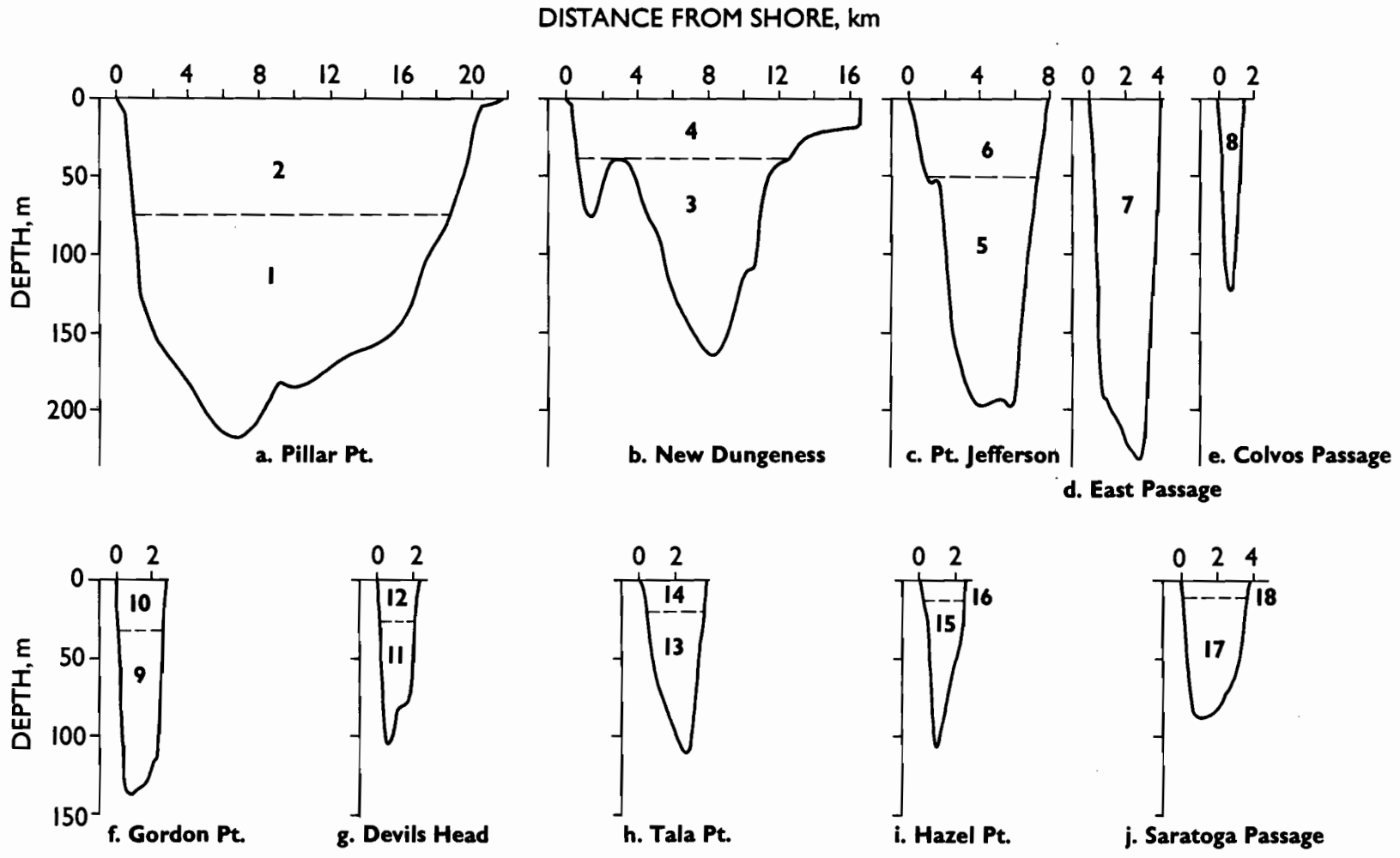

Figure 4. The channel cross sections as seen looking seaward showing the reach layers. The vertical distortion is 83:1.

the signal from a three-month moving average of the observations and the noise from the residuals. The uncertainty in the three-month mean comes from the variance of the residuals plus some systematic error introduced by the moving average process. The twelve-month average is the arithmetic mean of the three-month averages, and its uncertainty stems from the uncertainty in the three-month means via the first order perturbation technique known as the method of propagation of errors. The details are given in the Appendix.

Throughout this work overall averages will be tabulated for the period 15 February 1953 through 15 March 1955. This is the common interval over which every reach has sufficient, simultaneous salinity data to form annual moving averages. The data actually extend six months on either side of this interval in order to form annual averages. For some reaches, e.g. Point Jefferson, the data span is substantially longer, as will be shown in the graphs.

2.4 Error Analysis

When possible any data analysis or model should include error estimates so that the results can be put into perspective. The present work requires an error analysis of Knudsen's relations (7) and the flux-weighted salinities (11) that go into them. To investigate the effects of uncertainties on (11) we take the first variation Δ to give

$$\begin{aligned}
\Delta S_i = {} & \frac{\overline{\rho}}{Q_i} \int_{z_1}^{z_2} \Delta\overline{S}\ \underset{\sim}{\overline{u}}\cdot\underset{\sim}{n}\ w\ dz \\
& + \frac{\overline{\rho}}{Q_i} \int_{z_1}^{z_2} \left(\overline{S}-S_i\right) \Delta\underset{\sim}{\overline{u}}\cdot\underset{\sim}{n}\ w\ dz \\
& + \frac{\overline{\rho}}{Q_i} \int_{z_1}^{z_2} \left(\overline{S}-S_i\right) \underset{\sim}{\overline{u}}\cdot\underset{\sim}{n}\ \Delta w\ dz \\
& - (-1)^i \frac{\overline{\rho}}{Q_i} \left(\overline{S}-S_i\right) \underset{\sim}{\overline{u}}\cdot\underset{\sim}{n}\ w \Big|_{z_0} \Delta z_0 \quad + \cdots
\end{aligned} \tag{14}$$

where z_0 is the depth-of-no-net-motion between landward- and seaward-flowing layers, i.e. $z_0 = z_1$ for lower, landward-flowing layers and $z_0 = z_2$ for upper, seaward-flowing layers. Terms higher than first order are neglected. The flux-weighted salinity is insensitive to errors in the depth-of-no-net-motion since $\underset{\sim}{u}\cdot\underset{\sim}{n} = 0$ there, and the last term in (14) vanishes. The first three terms represent contributions to the error due to uncertainties in the mean salinity $\Delta\overline{S}$, mean velocity $\Delta\underset{\sim}{\overline{u}}\cdot\underset{\sim}{n}$ and channel width Δw. Squaring (14) and averaging yields the following equation for the flux-weighted salinity variance

$$\overline{\Delta S_i^2} \le \left[\frac{\overline{\rho}}{Q_i}\int_{z_1}^{z_2}\overline{(\Delta\overline{S})^2}^{1/2}\,\overline{\underset{\sim}{u}}\cdot\underset{\sim}{n}\;w\;dz + \frac{\overline{\rho}}{Q_i}\int_{z_1}^{z_2}(\overline{S}-S_i)\overline{(\Delta\overline{\underset{\sim}{u}}\cdot\underset{\sim}{n})^2}^{1/2}\;w\;dz\right]^2$$

$$+\left[\frac{\overline{\rho}}{Q_i}\int_{z_1}^{z_2}(\overline{S}-S_i)\,\overline{\underset{\sim}{u}}\cdot\underset{\sim}{n}\,\overline{(\Delta w)^2}^{1/2}\,dz\right]^2 + \cdots$$

$$\approx \left[\frac{\overline{\rho}}{Q_i}\int_{z_1}^{z_2}\overline{(\Delta\overline{S})^2}^{1/2}\,\overline{\underset{\sim}{u}}\cdot\underset{\sim}{n}\;w\;dz\right]^2 + \left[\frac{\overline{\rho}}{Q_i}\int_{z_1}^{z_2}(\overline{S}-S_i)\overline{(\Delta\overline{\underset{\sim}{u}}\cdot\underset{\sim}{n})^2}^{1/2}\;w\;dz\right]^2 \qquad (15)$$

$$+\left[\frac{\overline{\rho}}{Q_i}\int_{z_1}^{z_2}(\overline{S}-S_i)\,\overline{\underset{\sim}{u}}\cdot\underset{\sim}{n}\,\overline{(\Delta w)^2}^{1/2}\,dz\right]^2 + \cdots$$

where we have assumed that errors in the mean salinity and current are uncorrelated with errors in the channel widths. The first step in (15) represents a strict upper bound on the first-order error in that salinity and velocity errors are assumed to be fully self- and cross-correlated even after depth averaging. The second step is an approximation in which possible cross-correlations between the salinity and velocity errors are neglected. We lack long-term, simultaneous salinity and velocity observations to test this approximation, but we feel that it is justified especially since the remaining terms represent upper bounds. In the worst case the neglected cross terms could double the variance leading to flux-weighted salinity error bars $\left(\pm\overline{(\Delta S_i)^2}^{1/2}\right)$ which are at most a factor of $2^{1/2}$ larger than those calculated. This is unlikely.

The variance in the flux-weighted salinity has the potential for being not much greater than the variance in the time-mean salinity. If the uncertainty in $\overline{S}$ were independent of depth, then it could be brought outside the first integral and the first term in (15) would equal $\overline{(\Delta S_i)^2}^{1/2}$. For layers in which $\overline{S}$ varies little with depth, S_i approaches $\overline{S}$ and the second term approaches zero. Alternatively, if $\overline{(\Delta\overline{\underset{\sim}{u}}\cdot\underset{\sim}{n})^2}^{1/2}$ is simply proportional to $\overline{\underset{\sim}{u}}\cdot\underset{\sim}{n}$ over an entire layer, then again the second term vanishes. The third term in (15) representing the effects of channel-width error as interpolated from navigational charts is independent of and usually negligible compared to the other terms. If the errors are proportional to the channel width, the integral vanishes.

To find the effect of salinity and runoff errors on the transports we apply the method of propagation of errors (A16) to Knudsen's equations (11) setting j = 1 without loss of generality to give

$$\overline{\Delta Q_1^2} = Q_1^2 \left[\frac{\overline{\Delta S_1^2}}{(S_1-S_2)^2} - 2\frac{S_1}{S_2}\frac{\overline{\Delta S_1\,\Delta S_2}}{(S_1-S_2)^2} + \frac{S_1^2}{S_2^2}\frac{\overline{\Delta S_2^2}}{(S_1-S_2)^2} + \frac{\overline{\Delta R_{1\Sigma}^2}}{R_{1\Sigma}^2} \right. \tag{16}$$

$$\left. + \frac{2}{S_2(S_1-S_2)R_{1\Sigma}} \left(S_1\,\overline{\Delta S_2\,\Delta R_{1\Sigma}} - S_2\,\overline{\Delta S_1\,\Delta R_{1\Sigma}} \right) \right] + \cdots$$

$$\overline{\Delta Q_2^2} = Q_2^2 \left[\frac{S_2^2}{S_1^2}\frac{\overline{\Delta S_1^2}}{(S_1-S_2)^2} - 2\frac{S_2}{S_1}\frac{\overline{\Delta S_1\,\Delta S_2}}{(S_1-S_2)^2} + \frac{\overline{\Delta S_2^2}}{(S_1-S_2)^2} + \frac{\overline{\Delta R_{1\Sigma}^2}}{R_{1\Sigma}^2} \right.$$

$$\left. + \frac{2}{S_2(S_1-S_2)R_{1\Sigma}} \left(S_1\,\overline{\Delta S_2\,\Delta R_{1\Sigma}} - S_2\,\overline{\Delta S_1\,\Delta R_{1\Sigma}} \right) \right] + \cdots$$

The error cross-product terms require laborious calculation. To simplify we assume that fluctuations in the landward- and seaward-flowing salinities are correlated, i.e.

$$\overline{\Delta S_1\,\Delta S_2} = \overline{\Delta S_1^2}^{1/2}\,\overline{\Delta S_2^2}^{1/2}, \tag{17}$$

since the layers are usually superposed and observed simultaneously. To achieve an upper bound on the transport errors the salinity-runoff cross-terms can be neglected. To see this first assume that the terms are negatively correlated

$$\overline{\Delta S_1\,\Delta R_{1\Sigma}} = -\,\overline{\Delta S_1^2}^{1/2}\,\overline{\Delta R_{1\Sigma}^2}^{1/2},$$

$$\overline{\Delta S_2\,\Delta R_{1\Sigma}} = -\,\overline{\Delta S_2^2}^{1/2}\,\overline{\Delta R_{1\Sigma}^2}^{1/2}, \tag{18}$$

which means that higher-than average runoff leads to freshening and vice versa. The factors in (16) become

$$S_1\,\overline{\Delta S_2\,\Delta R_{1\Sigma}} - S_2\,\overline{\Delta S_1\,\Delta R_{1\Sigma}} = -\left(S_1\,\overline{\Delta S_2^2}^{1/2} - S_2\,\overline{\Delta S_1^2}^{1/2} \right) \overline{\Delta R_{1\Sigma}^2}^{1/2} \le 0 \tag{19}$$

since landward-flowing S_1 is greater than seaward-flowing S_2, and the salinity variance in the seaward-flowing, upper layer is always observed to exceed that of the lower layer. Therefore the terms in (19) reduce the error in (16). From (7), (17), and (18) equation (16) simplifies to

$$\overline{\Delta Q_1^2} \le \frac{\left(S_2\,\overline{\Delta S_1^2}^{1/2} - S_1\,\overline{\Delta S_2^2}^{1/2} \right)^2}{(S_1 - S_2)^4} R_{1\Sigma}^2 + \frac{S_2^2}{(S_1 - S_2)^2}\,\overline{\Delta R_{1\Sigma}^2} + \cdots$$

$$\overline{\Delta Q_2^2} \leq \frac{\left(S_2\,\overline{\Delta S_1^2}^{1/2} - S_1\,\overline{\Delta S_2^2}^{1/2}\right)^2}{(S_1 - S_2)^4}\,R_{1\Sigma}^2 + \frac{S_1^2}{(S_1 - S_2)^2}\,\overline{\Delta R_{1\Sigma}^2} + \cdots \qquad (20)$$

The minus sign in the first term of (20) shows that flux-weighted salinity error contributions tend to cancel in the transport errors.

The standard error is a measure of the uncertainty in a moving average. This within-year error is due to seasonal and random fluctuations. When several moving averages are averaged together to form an overall mean its appropriate error measure is the standard deviation of the population of moving averages as calculated from a model II analysis of variance (Brownlee, 1984; Snedecor and Cochran, 1980). This includes contributions from the within-year errors and from the between-year errors due to climatic change. Account must be taken of the fact that the moving-average process produces self-correlated time series when the temporal separation is less than the averaging interval. Therefore fewer independent estimates exist for constructing the overall average. As already mentioned, overall means will be tabulated for the interval 15 February 1953 through 15 March 1955. However, tabulated overall standard deviations will be from longer time intervals where the length of the data time series permit to increase the sample size.

3. REACHES AND MIXING ZONES

A reach is defined to be a two-layered segment of an estuary in which mass is transported principally by longitudinal advection when the flow is averaged over an appropriate time interval (I). Horizontal turbulent transport and vertical mean advective and turbulent transport are neglected. In this idealization, the reach layers exchange mass only in mixing zones where turbulent effects may dominate.

The boundaries between reaches and mixing zones depend upon several factors. The goal is to place the boundaries such that sills, reach intersections and river mouths are within mixing zones, and each reach has a long-term salinity and current meter station near its center. It is important that each station be representative of its reach. To achieve this, the seaward-flowing salinity there must result solely from a mixture of landward-flowing seawater and of fresh water that has entered the reach landward of the station.

The actual length of a reach will not affect the transport computations. If vertical transport between prospective reach layers is judged to be significant, its effect can always be reduced by shrinking the reach length to zero if necessary while centering on the salinity and current stations. However, when it comes to considering flushing times, the length will be important because the reach-layer transit time is defined (I.91) as the ratio of the layer mass to the mass flux and is directly proportional to the reach length.

In the present study we divide the Strait of Juan de Fuca/Puget Sound system into nine reaches and nine mixing zones (Figures 1 and 2). The reaches are named after nearby landmarks

and numbered sequentially beginning in the Strait of Juan de Fuca and increasing up the main axis of Puget Sound, then into Hood Canal and finally into Saratoga Passage. Each mixing zone bears the index of the reach located immediately seaward.

The channel cross-sections narrow and shoal in progression up the axis (Figure 4). The layer areas decrease from 1.61 km^2 for the lower layer A_1 off Pillar Point to 0.03 km^2 for the upper layers off Hazel Point A_{16} and in Saratoga Passage A_{18} (Table 1).

Pillar Point reach 1 occupies the outer Strait of Juan de Fuca. It is bounded to the west by the Pacific Ocean and to the east by a line extending north from Port Angeles (Figure 1). It is a flooded, U-shaped, glacial valley (Figure 4) with depths at midchannel decreasing from 250 m to 165 m as one moves landward (Figure 2). The inflowing bottom water of layer 1 is the source of all the sea salt in Puget Sound. Mixing zone 1 separates Pillar Point reach from New Dungeness reach with a convoluted sill which runs approximately from Port Angeles to Victoria. The typical sill depth is 90 m, but it dips to 120 m within a narrow 1 km gap (See Ebbesmeyer *et al.*, 1984, Figure 3.1, for a map of sill locations). This mixing zone provides a convenient way to introduce the substantial runoff from the Fraser River whose location is shown in the inset map of Figure 1a. Since it is not our intention to model the circulation in Haro Strait and the Strait of Georgia, but simply to provide a connection to the Pacific Ocean for Puget

TABLE 1. The cross-sectional areas A_i of the reach layers.

	Reach Layer	A_i km^2
1	Pillar Pt. lower	1.615
2	Pillar Pt. upper	1.433
3	New Dungeness lower	0.652
4	New Dungeness upper	0.580
5	Pt. Jefferson lower	0.606
6	Pt. Jefferson upper	0.354
7	East Passage	0.698
8	Colvos Passage	0.117
9	Gordon Pt. lower	0.223
10	Gordon Pt. upper	0.085
11	Devils Head lower	0.110
12	Devils Head upper	0.064
13	Tala Pt. lower	0.180
14	Tala Pt. upper	0.071
15	Hazel Pt. lower	0.111
16	Hazel Pt. upper	0.032
17	Saratoga Passage lower	0.215
18	Saratoga Passage upper	0.035

Sound, we include both straits and their runoff in mixing zone 1. Following Waldichuk (1957) we neglect flow through the Strait of Georgia; hence mixing zone 1 is assumed to be closed at the far northern end (not shown in Figure 1).

New Dungeness reach 2 occupies the inner Strait of Juan de Fuca. It is about 170 m deep at midchannel (Figure 4). This reach is not well defined geographically since the deep east-west channel branches northward into Haro Strait. At its lower depths the salinity station is representative of the most saline water available to enter Puget Sound. Mixing zone 2 extends from Rosario Strait southward into Admiralty Inlet and then northward past the Snohomish River to the mouth of the Stillaguamish River. Net surface currents in Rosario Strait have been inferred to flow both northward (Thomson, 1981) and southward (Ebbesmeyer *et al.*, 1984) based upon sparse data. We have neglected this flow because of the uncertainty. If in fact it carries substantial Fraser River runoff southward, diluting the surface outflow in layer 4, then by Knudsen's equations (7) its neglect will lead to an underestimate of the transport in reach 2. In Admiralty Inlet, the primary entrance to Puget Sound, several reaches join the mixing zone in a multiple junction. Minimum midchannel depths of 65 m and strong tidal currents promote vigorous vertical mixing there.

Layers 5 and 6 comprise Point Jefferson reach 3 near Seattle (Figure 2). It is over 200 m deep (Figure 4) but does not terminate in a sill at its southern end (See Burns, 1985 for contour maps of Puget Sound). Instead, mixing zone 3 is formed by the intersection of East and Colvos Passages, layers 7 and 8, with fresh water entering from the Duwamish River and the Lake Washington Ship Canal. There is a 50-meter-deep sill at the northern end of Colvos Passage which itself is 125 m deep, but East Passage is an unobstructed southward continuation of the Puget Sound main basin with a depth of over 200 m (Figure 2).

Layers 7 and 8 in reach 4 are unique in that they are juxtaposed with Vashon Island separating them rather than superposed (Figures 1b and 4). There is a clockwise mean circulation around Vashon Island (Farmer and Rattray, 1963). On the west side in Colvos Passage the mean flow is seaward from surface to bottom and the channel cross-section is small enough (Figure 4) that the mean flow can overcome the flooding tidal current during most of the tidal cycle (Larsen, Shi and Dworski, 1977), a fact utilized by early navigators (United States Coast and Geodetic Survey, 1889). Water in East Passage flows landward in the mean, but there is evidence (Bretschneider, Cannon, Holbrook and Pashinski, 1985) of a shallow (~10 m), weak (~1000 m^3/s) seaward flow at the surface which we shall neglect. The Puyallup River enters mixing zone 4, and strong tidal currents in the 50- to 80-meter-deep Narrows vigorously agitate the flow.

South of the Narrows lies 165-meter-deep Gordon Point reach 5 (Figure 1b). At its southern end the bottom shoals to 35 m in mixing zone 5 near the Nisqually River delta (Figure 2).

Landwardmost reach 6 in southern Puget Sound begins at Devils Head where the depth is 105 m (Figure 2). Runoff enters at the heads of several inlets landward of this site with the Deschutes River at Olympia being the single largest source (Figure 1b).

To the west of Puget Sound's main basin is Hood Canal, a natural, glacially carved fjord (Figure 1b). Reach 7 at its northern end is represented by the Tala Point hydrographic station. This 115-meter-deep station is nearly within the Admiralty Inlet mixing zone and may not be entirely representative of the reach, but we use it for lack of an alternative station having a long salinity record. To the south of Tala Point reach lies mixing zone 7 which is about 50 m deep at its shallowest, midchannel location (Figure 2).

Hazel Point reach 8 in Hood Canal is over 150 m deep along most of its length with maximum depths of about 175 m (Figure 2). Its deep circulation is slow and occasionally leads to hypoxia in mixing zone 8 at the landward end (Collias, McGary and Barnes, 1974). River runoff from the Olympic Mountains to the west is distributed along its length (Figure 1b).

The ninth reach is comprised of layers 17 and 18 in Saratoga Passage (Figure 1b). This reach is 165 m deep at its southern end where it lacks a sill, and it shoals to 50 m at its northern end joining mixing zone 9 (Figure 2). This mixing zone is unique in several regards: (1) It receives inflow from the Skagit River, the largest within Puget Sound. (2) At its northern end narrow, 12-meter-deep Deception Pass provides a "leak" to mixing zone 2. (3) Instantaneous tidal currents within the Pass are the strongest in Puget Sound, exceeding 4 m/s at times and thus are able to homogenize the water there (Collias, Barnes and Lincoln, 1973).

4. RUNOFF

Fresh water is one convenient tracer of the circulation in Puget Sound. Its rate of input is usually measured with river flow gauges. However, some principal rivers are often ungauged, and for others only a portion of their drainage basins are sampled. Therefore some method is needed to relate ungauged to gauged river discharges.

For the Strait of Georgia comprising most of mixing zone 1, Waldichuk (Table XV, 1957) has provided a list of monthly correction factors to be applied to the Fraser River discharge at Hope, B.C., in order to estimate the total runoff.

For Puget Sound, Lincoln (1977) has developed a technique similar to Waldichuk's. The basic idea is to compensate for each ungauged drainage area by identifying suitable gauged reference streams and approximating the ungauged flow by the product of the gauged flow and the ungauged-to-gauged area ratio. A suitable stream is one whose gauged drainage basin is comparable to the ungauged area in terms of elevation, terrain, rainfall and evapotranspiration. Lincoln chose 20 reference gauging stations and analyzed the runoff of the 14 major watersheds (Gladwell and Mueller, 1967) tributary to Puget Sound (Figure 5) for October 1974 to September 1975. Unfortunately 10 of Lincoln's (1977) reference stations did not operate during the period of interest, the mid 1950's. To adapt his method we have chosen 18 USGS gauging stations

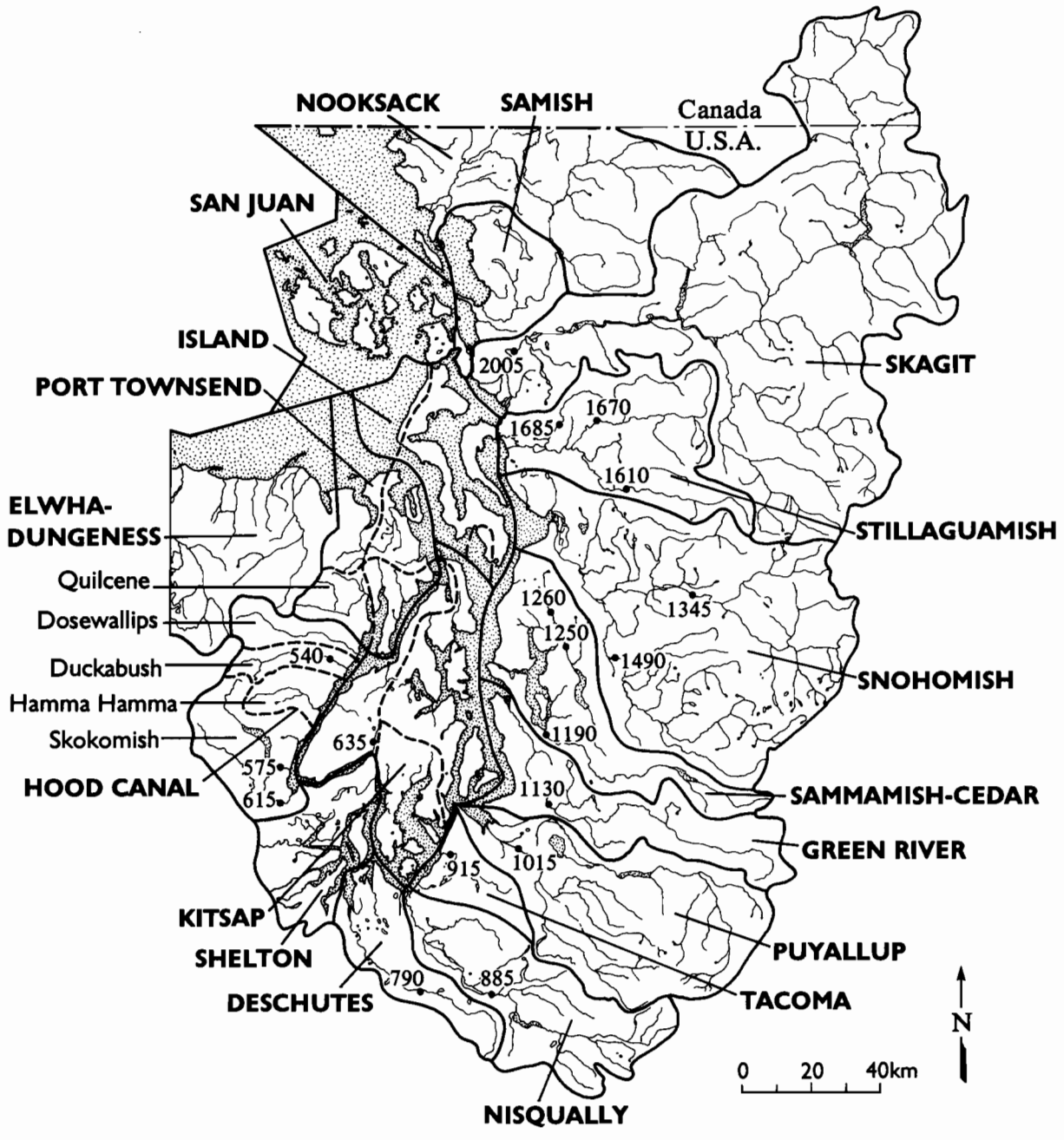

Figure 5. The Puget Sound watersheds. Bold lines denote the watershed boundaries of Gladwell and Mueller (1967), dashed lines denote the approximate subdivisions of Lincoln (1977), and dots with numbers mark the sites and indices of USGS (1964) gauging stations. (Map adapted from University of Washington, Figure 3-1, 1953.)

(United States Geological Survey, 1964) as shown in Figure 5 and have computed the appropriate ungauged-to-gauged-area ratios. Table 2 gives the resulting coefficients. As an example from the table, the Skagit River runoff into Whidbey Basin is given from columns 1, 2 and 7 by:

$$1.00 \times (\text{gauged flow of the Skagit R. near Mt. Vernon})$$
$$+ 1.31 \times (\text{gauged flow of Pilchuck Crk. near Bryant}).$$

Three errors in Lincoln's (1977) method have been corrected. The drainage area for the Snohomish watershed should be 1852 square miles (Gladwell and Mueller, 1967), not 1630 square miles. Lincoln subdivided the Hood Canal and Port Townsend watersheds of Gladwell and Mueller (1967) into 4 component watersheds each after the University of Washington (1953) (Figure 5). The Quilcene River watershed was added to Hood Canal, but Lincoln failed to subtract its area from Port Townsend's watershed. Finally, a significant diversion of the North Fork of the Skokomish River directly into Hood Canal by Cushman Dam No. 2 was overlooked.

Table 3 lists the apportionment of the watershed runoff into the various mixing zones. Since our theoretical framework allows runoff to be introduced only into mixing zones, some compromises are necessary. In mixing zone 1 we neglect inputs from the shores of the Strait of Juan de Fuca compared to the substantial input from the Strait of Georgia. Also neglected are small inputs into mixing zone 2 from those parts of the Port Townsend, Island and San Juan watersheds which border the Strait of Juan de Fuca. In Hood Canal, although the runoff is distributed along the entire length of reach 8, it has been consolidated into mixing zone 8. This is partially justified by the small longitudinal salinity gradients observed there (Collias *et al.*, 1974).

The monthly mean flow for the Fraser River (Station 8MF5 at Hope, British Columbia) was obtained from Canadian records (Canada, 1955, 1957, 1959) for the period October 1950 to September 1956. Similar data for the other gauging stations in Table 1 were obtained from USGS records (United States Geological Survey, 1964). Data for Pilchuck Creek were not available during October 1951 to September 1952. A linear least squares multiple regression between Pilchuck Creek and several other gauging stations for the previous 1 and following 4 years yielded a very good fit (96% of the variance accounted for by the regression, significance level = 0.0001; Snedecor and Cochran, 1980) which was used to predict the flow over the missing period.

Time series of the twelve-month moving average runoff R_i entering each mixing zone are shown in Figure 6. The Strait of Juan de Fuca/Puget Sound system differs from a classical fjord in that the bulk of the runoff enters near the mouth from the Fraser River in mixing zone 1 rather than at the head. The same is true of Puget Sound itself, where mixing zones 2 and 9 dominate owing to the Stillaguamish/Snohomish and Skagit Rivers, respectively. The runoff entering mixing zones 3 through 6 along the main axis is highly correlated (correlation coefficient

TABLE 2. Coefficients for calculating the runoff into the Puget Sound basins from USGS gauging stations (adapted from Lincoln, 1977).

Principal Puget Sound Basin	Watershed	Area (sq. mi.)	Gauging Station	Station Number	Gauged Area (sq. mi.)	Coefficient
Admiralty Inlet	Island	9	Pilchuck Crk. near Bryant	1685	50	0.18
	Port Townsend	60	Pilchuck Crk. near Bryant	1685	50	1.21
Whidbey Basin	Skagit	3125	Skagit R. near Mt. Vernon	2005	3060	1.00
			Pilchuck Crk. near Bryant	1685	50	1.31
	Stillaguamish	707	S. Fork Stillaguamish R. near Granite Falls	1610	119	1.00
			N. Fork Stillaguamish R. near Arlington	1670	269	1.00
			Pilchuck Crk., near Bryant	1685	50	6.42
	Snohomish	1852	Skykomish R. near Gold Bar	1345	535	1.00
			Snoqualmie R. near Carnation	1490	608	1.00
			Pilchuck Crk. near Bryant	1685	50	14.27
	Island	163	Pilchuck Crk. near Bryant	1685	50	3.28
Main Basin	Sammamish-Cedar	647	Cedar R. at Renton	1190	197	1.00
			Sammamish R. near Redmond	1250	148	1.00
			North Crk. near Bothell	1260	24	12.58
	Green	517	Green R. near Auburn	1130	382	1.00
			Sammamish R. near Redmond	1250	148	0.91
	Puyallup	1030	Puyallup R. at Puyallup	1015	948	1.00
			Chambers Crk. below Leach Crk. near Steilacoom	915	104	0.79
	Kitsap	222	Union R. near Belfair	635	19	11.68
South Sound	Tacoma	193	Chambers Crk. below Leach Crk. near Steilacoom	915	104	1.86
	Nisqually	716	Nisqually R. near McKenna	885	445	1.00
			Deschutes R. near Rainier	790	90	3.01
	Deschutes	270	Deschutes R. near Rainier	790	90	3.00
	Kitsap	222	Union R. near Belfair	635	19	11.68
	Shelton	358	Deschutes R. near Rainier	790	90	3.98
Hood Canal	Skokomish	286	Skokomish R. near Potlatch	615	230	1.00
			N. Fork Skokomish R. near Hoodsport	575	Diversion	1.00
			Deschutes R. near Rainier	790	90	0.62
	Hamma Hamma	102	Duckabush R. near Brinnon	540	67	1.52
	Duckabush	86	Duckabush R. near Brinnon	540	67	1.28
	Dosewallips	126	Duckabush R. near Brinnon	540	67	1.88
	Quilcene	101	Duckabush R. near Brinnon	540	67	1.51
	Port Townsend	139	Duckabush R. near Brinnon	540	67	2.07
	Kitsap	222	Union R. near Belfair	635	19	11.68

TABLE 3. Portions of the watershed runoff entering the mixing zones and their May 1951–December 1955 mean and standard deviation.

Mixing Zone	Principal Basin	Watershed	Portion	m^3/s
1	Strait of Georgia		1.0	4511.0 ± 534.6
2	Admiralty Inlet	Island	1.0	1.4 ± 0.2
		Port Townsend	1.0	9.6 ± 1.7
	Whidbey	Stillaguamish	1.0	136.5 ± 24.5
		Snohomish	1.0	335.2 ± 59.8
		Island	0.5	13.0 ± 2.3
	Main Basin	Kitsap	0.2	3.6 ± 0.8
3	Main Basin	Sammamish-Cedar	1.0	39.6 ± 8.6
		Green	1.0	44.7 ± 10.1
		Kitsap	0.6	10.8 ± 3.9
4	Main Basin	Puyallup	1.0	96.4 ± 16.7
		Kitsap	0.2	3.6 ± 0.8
	South Sound	Tacoma	0.5	2.9 ± 1.2
		Kitsap	0.5	9.0 ± 1.9
5	South Sound	Tacoma	0.5	2.9 ± 1.2
		Nisqually	1.0	75.1 ± 12.6
		Kitsap	0.1	1.8 ± 0.4
6	South Sound	Deschutes	1.0	23.1 ± 4.3
		Kitsap	0.4	7.2 ± 1.6
		Shelton	1.0	30.6 ± 5.7
7	Hood Canal	Port Townsend	1.0	26.4 ± 3.8
		Kitsap	0.3	5.4 ± 1.2
8	Hood Canal	Skokomish	1.0	62.7 ± 10.5
		Hamma Hamma	1.0	19.4 ± 2.8
		Duckabush	1.0	16.3 ± 2.4
		Dosewallips	1.0	24.0 ± 3.5
		Quilcene	1.0	19.3 ± 2.8
		Kitsap	0.7	12.6 ± 3.9
9	Whidbey	Skagit	1.0	489.3 ± 92.2
		Island	0.5	13.0 ± 2.3

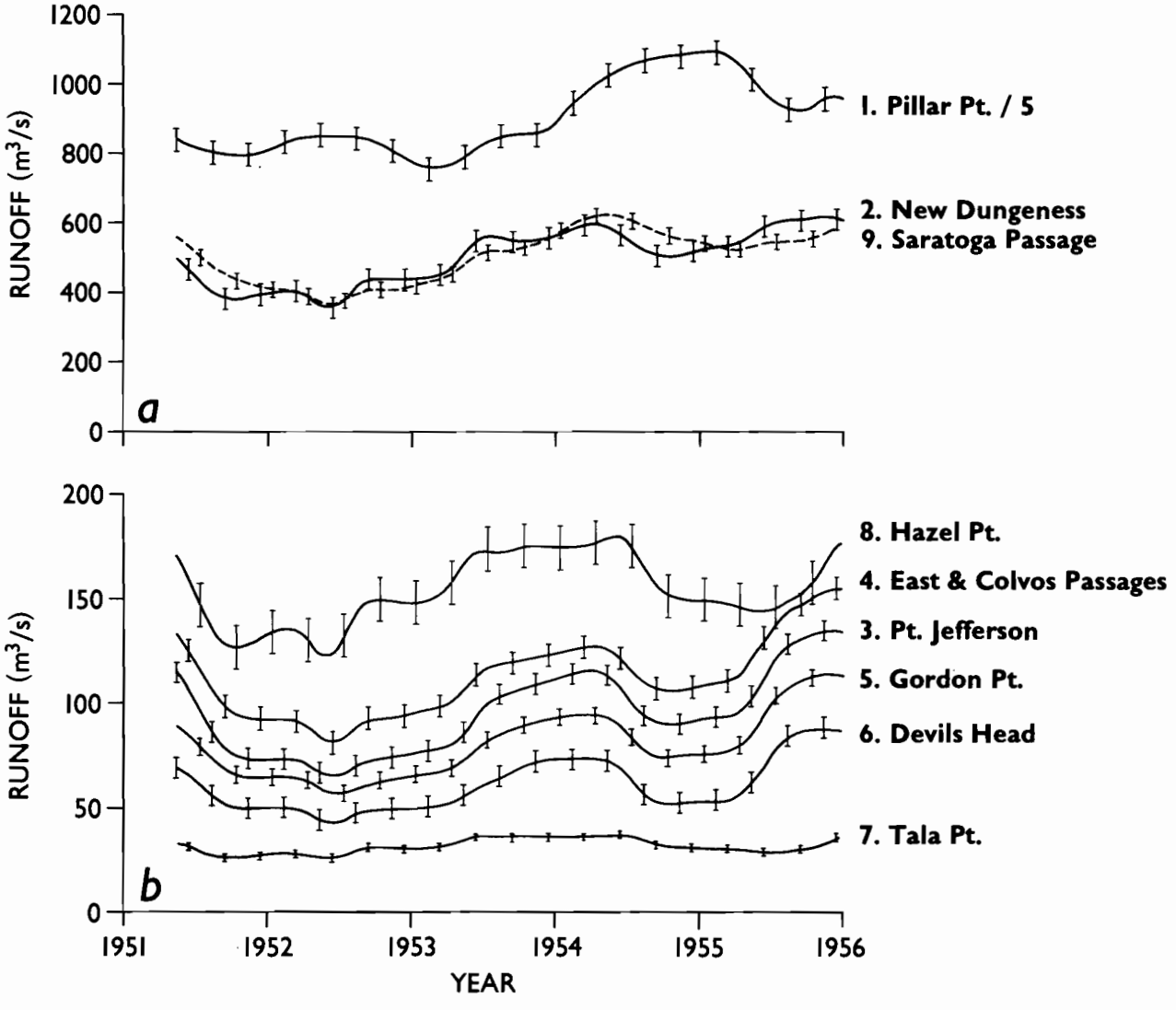

Figure 6. The annual mean runoff R_i entering each mixing zone of the Strait of Juan de Fuca and Puget Sound. Note the scaling for Pillar Point reach. The error bars represent the standard error of the mean.

$r \geq 0.97$, Table 4), due in part to common index gauging stations, but also due to common watershed characteristics. The headwaters are on the western slopes of the Cascade mountains, drain a small area relative to the size of a typical storm, and are at low enough elevation that precipitation falls mainly as rain. The Hood Canal runoff pattern, R_7 and R_8, is of the classical fjord type with the landwardmost river dominating.

Knudsen's equations (7) depend upon the cumulative runoff (Figure 7). Due to its cumulative nature this decreases monotonically by a factor of 100 as one moves landward up the axis of the Sound.

The overall means and standard deviations of the annual moving-average runoff are given in Table 5 for the period 15 February 1953 to 15 March 1955.

5. CURRENTS

The currents observed in Puget Sound from 1908 to 1980 have been indexed and tabulated by Cox *et al.* (1984). Measurement sites near hydrographic stations and reach centers were selected for this study (Figure 1 and Table 6). With the exception of reach 1 these are at midchannel. Most of the currents (90% of the total duration) were measured in the 1970's prior to 1979. At about this time the available, but sketchy, evidence suggests that the landward flow in reach 3 made a transition from mid-depth to bottom intensification (Ebbesmeyer *et al.*, 1989). This probably occurred in response to an enhanced salinity gradient across Admiralty Inlet mixing zone 2 due to a climatic shift from cool, wet conditions reminiscent of the 1950's to warm, dry conditions. This current signal has not been detected elsewhere, and currents from other periods have been used to provide better data coverage. The cumulative duration of the observations varies markedly between reaches, and some, such as Devils Head and Tala Point, are sparsely sampled (Table 7).

The direction of each cross-section normal vector is determined in a natural way from the current observations. We compute the vector mean current direction $\overline{\theta}$ measured from true North weighted by the record duration for both the landward- ($\overline{\theta}_{2j-1}$) and seaward-flowing ($\overline{\theta}_{2j}$) layers. The normal direction is usually set equal to the mean of $\overline{\theta}_{2j}$ and $\overline{\theta}_{2j-1} \pm 180°$ (Table 6). For the Gordon and Hazel Point reaches the normal directions are for the upper layers only. For the former the lower-layer composite record length was too short (15 d), and for the latter the mean current was too small (2 cm/s) to give reliable directions. The New Dungeness reach cross section lies along a line from Dungeness Spit to an offshore bank to avoid spanning a trough extending northward into Haro Strait (Figure 1a). At this section the currents are mainly influenced by Puget Sound thus minimizing the effect of Haro Strait.

The channel cross sections have been chosen to lie perpendicular to the normal vectors and either to pass through the current observation sites or between them and the salinity stations (Figures 1 and 4).

TABLE 4. Correlations between the annual mean runoff R_i.

	R_1	R_2	R_3	R_4	R_5	R_6	R_7	R_8	R_9
R_1	1								
R_2	0.57	1							
R_3	0.41	0.91	1						
R_4	0.37	0.88	0.99	1					
R_5	0.37	0.89	0.99	0.99	1				
R_6	0.26	0.85	0.98	0.97	0.99	1			
R_7	0.28	0.73	0.63	0.60	0.59	0.60	1		
R_8	0.28	0.78	0.71	0.68	0.67	0.68	0.99	1	
R_9	0.70	0.88	0.84	0.80	0.80	0.74	0.73	0.77	1

TABLE 5. The overall mean mixing zone runoff R_i, cumulative runoff $R_{i\Sigma}$ and their standard deviations.

Mixing Zone i	R_i (m^3/s)	$R_{i\Sigma}$ (m^3/s)
1	4731 ± 632	6372 ± 798
2	536 ± 81	1641 ± 271
3	99 ± 25	358 ± 85
4	115 ± 25	259 ± 61
5	82 ± 20	144 ± 36
6	62 ± 16	62 ± 16
7	35 ± 4	200 ± 25
8	166 ± 20	166 ± 20
9	546 ± 88	546 ± 88

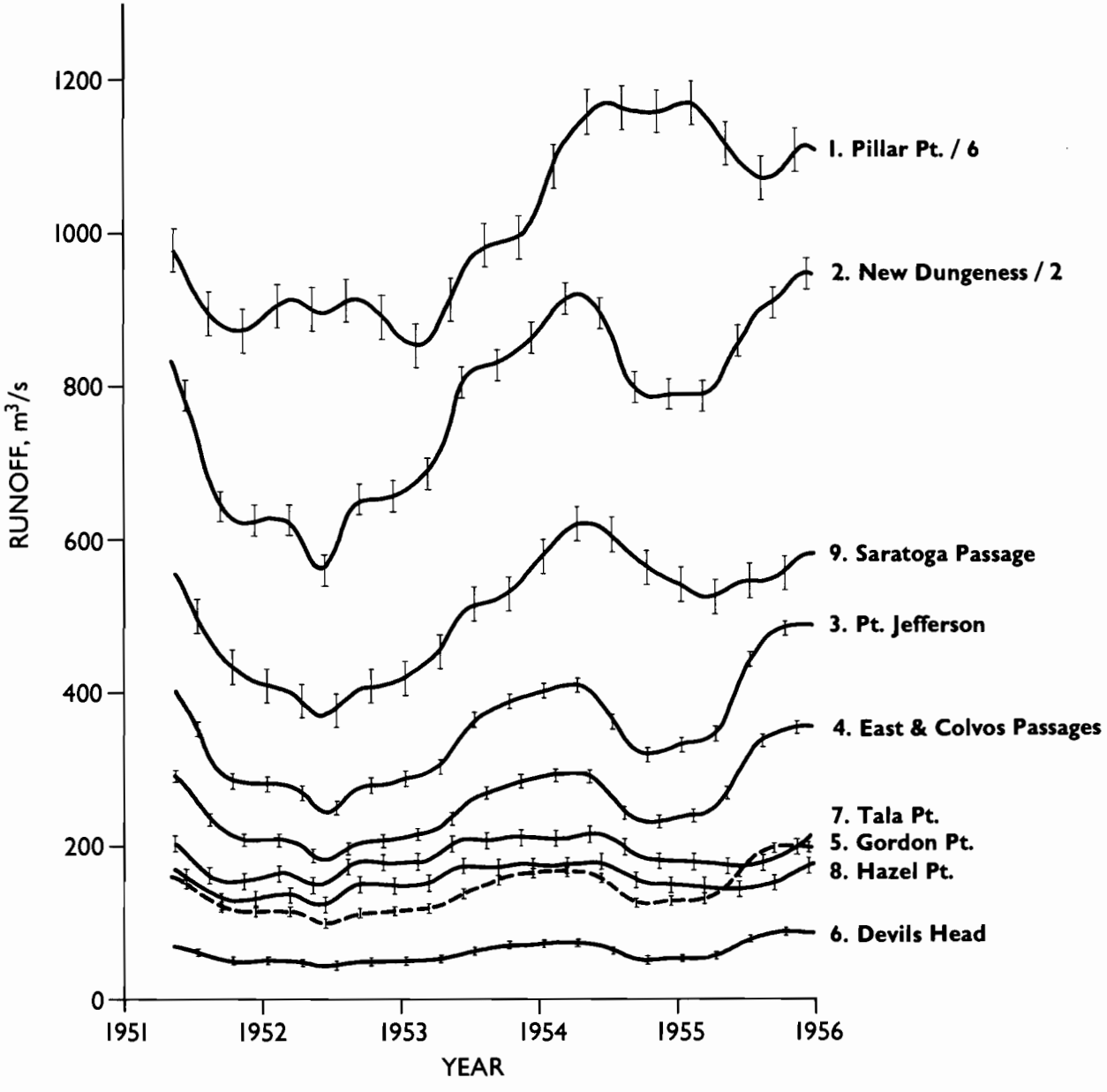

Figure 7. The annual mean cumulative runoff $R_{i\Sigma}$ entering the Strait of Juan de Fuca and Puget Sound landward of each reach. Note the scaling for Pillar Point and New Dungeness reaches.

TABLE 6. Sources and years of current observations and average directions of cross section unit normal vector $\underline{n}$.

Reach	Source and Station Number	Years of Observations	Direction (°T) (Average Directions of Upper/ Lower Layers)
1 Pillar Pt.	NOAA/NOS Stas. 96, 97, 98 (1975) & 96, 97 (1978) NOAA/PMEL Stas. JDF–12 to 16, ST–4 (1976) & MESA-N, MESA-S, ST-7 (1977)	1975–78	299 (290/308)
2 New Dungeness	NOAA/NOS Sta. 79 (1964) Holbrook *et al.* (1980), Stas. JDF-42, JDF-52, ST-10, ST-13	1964, 1978	308 (304/288)
3 Pt. Jefferson	Laird & Galt (1975) Cox *et al.* (1984), Sta. 146	1972–73, 1975–78	46 (33/59)
4 East Passage	*Ibid.*, Stas. 175, 176 Evans-Hamilton, Inc. (1983) Stas. 1, 7	1943, 1977, 1982–83	23 (–/23)
Colvos Passage	Cox *et al.* (1984) Stas. 195, 197, 199, 200, 201	1947, 1977	5 (5/–)
5 Gordon Pt.	*Ibid.*, Stas. 293, 295	1945, 1977–78	11 (11/322)
6 Devils Head	*Ibid.*, Stas. 317, 318	1945, 1978	164 (164/163)
7 Tala Pt.	*Ibid.*, Stas. 228, 230	1942, 1952, 1963, 1977–78	325 (323/327)
8 Hazel Pt.	*Ibid.*, Sta. 246	1942, 1978	8 (8/321)
9 Saratoga Passage	*Ibid.*, Stas. 28, 29	1943, 1970, 1977	165 (165/164)

TABLE 7. Inventory of current meter records and hydrographic casts.

Reach	Current Meter Records		Hydrographic Casts	
	Number	Cumulative Duration (d)	Number of Casts	Number of Samples
1 Pillar Pt.	43	1422	71	647
2 New Dungeness	15	1205	34	337
3 Pt. Jefferson	61	2843	126	1017
4 East Passage	16	717	41	449
Colvos Passage	12	254	38	302
5 Gordon Pt.	15	417	37	364
6 Devils Head	5	50	35	243
7 Tala Pt.	15	213	35	275
8 Hazel Pt.	4	85	37	294
9 Saratoga Passage	14	224	32	285
TOTAL	200	7430	486	4213

Each composite current profile is computed by a vertical least squares fit to the normal components $\bar{\underset{\sim}{u}} \cdot \underset{\sim}{n}$ of the velocity observations (Figure 8). The current record is linearly weighted by its duration to emphasize long time series. Hansen and Rattray (1965) gave a similarity solution for the velocity profile in the central regime of an estuary in which the longitudinal velocity is a cubic polynomial in the vertical coordinate, and the bottom velocity vanishes. These two conditions cannot always be satisfied realistically by a fit to the velocity data. When the profile is unrealistic or the highest order coefficient is insignificant, a quadratic suffices with little decrease in the goodness of fit. For some profiles the bottom velocity should be brought to zero in a thin boundary layer whose level of complexity is beyond the scope of this paper. In those cases a best fit is chosen, and the vanishing bottom velocity condition is relaxed. For still other profiles characteristic of a classical fjord with a shallow, surface outflow balanced by a slow, return flow spread over the deep lower layer, a polynomial fit is not appropriate due to the rapid decrease of velocity with depth. Here an exponential fit suffices.

In most instances the mean flow is two-layered with a seaward-flowing upper layer and a deeper return flow (Figure 8). In East Passage the flow is landward except for a very thin surface layer which may not be persistent, and which in any event has been neglected. In narrow Colvos Passage the current is seaward and much larger in order to balance the East Passage transport. The Hazel Point and Saratoga Passage current profiles which have exponential fits are nearest to those of a classical fjord.

The squared correlation coefficient of the regression r^2 exceeds 0.8 in most reaches thus indicating a good fit (Table 8). For Pillar Point reach the fit accounts for only 37% of the variance because the cross-channel variance has been lumped into the vertical fit. Currents there

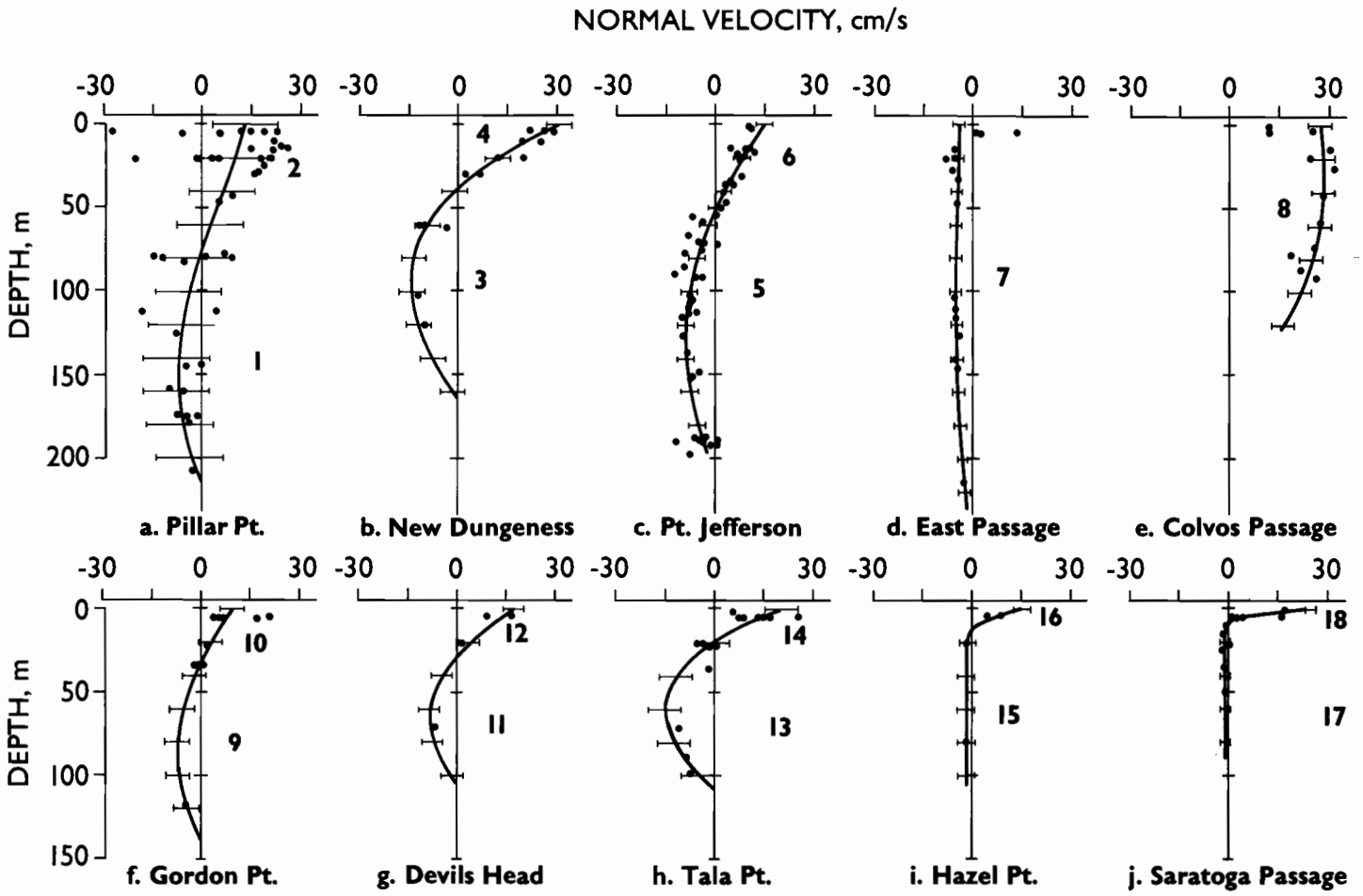

Figure 8. Composite vertical profiles of the velocity normal to each reach cross section (see Figure 1). The dots represent the observations, and the solid lines with error bars are the least squares fits. The profiles are two-layered except for East and Colvos Passages.

TABLE 8. Bottom depth D, regression equation and zero-crossing depth z_o for the normal velocity $\underset{\sim}{\bar{u}} \cdot \underset{\sim}{n}$ as a function of depth z (m), squared correlation coefficient r^2 and the standard error of the regression.

Reach	D(m)	$\underset{\sim}{\bar{u}} \cdot \underset{\sim}{n}$ (cm/s) =	z_o	r^2	error (cm/s)
1 Pillar Pt.	215	$0.2721\ (z-D) + 2.673 \times 10^{-3}\ (z-D)^2 + 5.232 \times 10^{-6}\ (z-D)^3$	74.5	0.37	10.10
2 New Dungeness	165	$0.3326\ (z-D) + 9.156 \times 10^{-4}\ (z-D)^2 - 1.359 \times 10^{-5}\ (z-D)^3$	38.3	0.94	3.79
3 Pt. Jefferson	196	$14.99 - 0.3709\ z + 1.441 \times 10^{-3}\ z^2$	50.2	0.87	2.48
4 East Passage	230	$-4.245 - 2.341 \times 10^{-2}\ z + 1.471 \times 10^{-4}\ z^2$	unidirectional	0.11	1.67
Colvos Passage	123	$27.07 + 8.941 \times 10^{-2}\ z - 1.491 \times 10^{-3}\ z^2$	unidirectional	0.33	3.49
5 Gordon Pt.	137	$0.2950\ (z-D) + 3.209 \times 10^{-3}\ (z-D)^2 + 3.943 \times 10^{-6}\ (z-D)^3$	31.5	0.62	3.66
6 Devils Head	104	$0.4467\ (z-D) + 5.882 \times 10^{-3}\ (z-D)^2$	28.3	0.94	3.05
7 Tala Pt.	110	$0.5199\ (z-D) + 2.767 \times 10^{-3}\ (z-D)^2 - 3.357 \times 10^{-5}\ (z-D)^3$	19.8	0.83	4.97
8 Hazel Pt.	106	$-1.541 + 16.74 \exp(-0.1850\ z)$	13.0	0.90	2.50
9 Saratoga Passage	88	$-0.8410 + 25.73 \exp(-0.3787\ z)$	9.1	0.94	1.45

are complicated by landward intrusions of oceanic water on the southern side of the channel which adds to the variance (Cannon and Holbrook, 1981; Holbrook, Cannon and Kachel, 1983; Proehl and Rattray, 1984; Cannon and Bretschneider, 1986). The fit in East Passage has one of the lowest root-mean-square errors but also the lowest value of r^2. This is because the data are nearly uniform from top to bottom except for a thin surface layer. The fit passes through the majority of the data near the mean very well but does not pass through the few surface values which contribute most of the variance. The fit is adequate for our purposes and shows the inadequacy of r^2 as a measure in this case. A similar argument holds for Colvos Passage.

6. SALINITY

The primary source of salinity data stems from the University of Washington Department of Oceanography's field program (Barnes and Collias, 1954a-c, 1956a-c), and supplementary data for the Strait of Juan de Fuca comes from Canadian studies (Joint Committee on Oceanography, 1955). We use data from station numbers 114, 141, 305, 320, 353, 405, 407, 501, 510 and 612 for January 1951 through February 1956 as indexed by Collias (1970). Not all of the time series commence in the same month, and large temporal gaps appear at the outset. Herein, no time series is used until the initial sampling interval decreases to four months or less. In total 4213 salinity observations were taken in 486 hydrographic casts (Table 7) at the sites marked in Figure 1.

The salinities were observed at selected depth intervals ranging from 5 m near the surface to 25 m at depth. For the present analysis the data have been interpolated with cubic splines to 5-meter intervals except for the shallow surface layers of Hazel Point and Saratoga Passage, where 1-meter intervals were used. Typographic errors in the data reports and data entry errors were detected by comparing plots of the spline-interpolated profiles and the data points. Punched cards on file at the University of Washington School of Oceanography contained rare chlorinity and salinity mismatches. Standard oceanographic conversions revealed that the chlorinities were correct and agreed with the salinities of the published data reports.

The overall mean salinity profiles and their standard errors are shown in Figure 9 for each reach. In general the salinity decreases as one moves landward from the Strait of Juan de Fuca up any axis of the Sound. Saratoga Passage is the most highly stratified due to the Skagit River which enters near its head. The next steepest vertical gradient appears at Hazel Point, but Pillar Point possesses a greater surface-to-bottom salinity difference owing to the influence of the Fraser River. The vertical salinity gradients as shown do not vanish at the bottom. This is due to cubic spline extrapolation from near-bottom values and should not be construed as a salt flux from the sediments. This artifact has a negligible effect on our results.

To calculate the flux-weighted salinity the integrands in (11) were interpolated to equispaced depths and integrated using Simpson's rule. The overall-means of the resulting two-layer salinities are plotted in Figure 9 along with the overall-means of the vertical profiles.

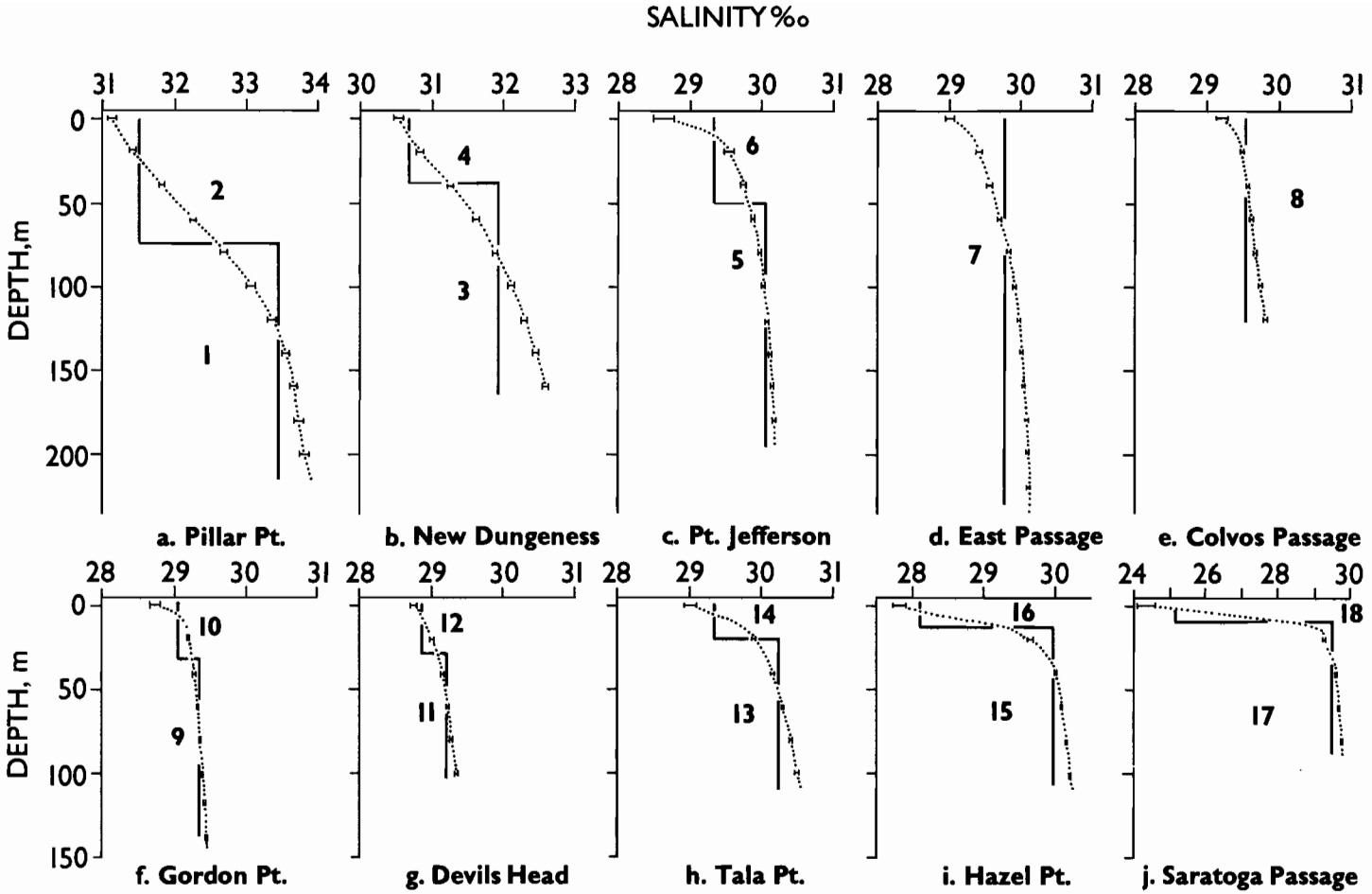

Figure 9. Vertical profiles of the mean (dotted lines) and flux-weighted (solid lines) salinities for each reach layer as numbered. The error bars correspond to the standard error of the mean. These profiles are the average of all the annual means which were tabulated monthly. The scaling is identical except for Saratoga Passage which is halved. The origins are shifted to allow for the landward decrease of salinity.

Given the salinity profiles alone it would be difficult to assign the depth of the interface between landward- and seaward-flowing layers. At several sites, for instance layers 5 and 6 off Point Jefferson and layers 9 and 10 off Gordon Point, the depth of the halocline and the level-of-no-net-motion differ by tens of meters (Figures 8 and 9). At other sites, for instance layers 1 and 2 off Pillar Point and layers 3 and 4 off New Dungeness, the depth of the halocline is ambiguous since the salinity gradient is gradual.

The calculation of the flux-weighted salinities in East and Colvos Passages presented some special problems. In the other reaches the layer pairs were sampled nearly simultaneously since they are superimposed and each hydrographic cast penetrated both layers. East and Colvos Passages are separate geographical locations (Figure 1) which usually were sampled within a few hours of one another. Unfortunately during 5 of 37 cruises, samples were collected in one Passage only. During temporal interpolation these missing samples can cause the flux-weighted salinity differences to approach zero in a non-physical way. To remedy this we completed the time series for each layer by inserting missing values using a linear regression of each layer's flux-weighted salinity against the other's. The equation of the linear regression with the error distributed amongst both time series (Larsen, 1980) is

$$S_8 = 1.208\ S_7 - 6.43\ ‰ \qquad (21)$$

with $r^2 = 0.96$. The flux-weighted salinities were time-averaged after the insertion of the missing values.

Time series of the annual mean flux-weighted salinities (Figure 10) show that the landward-flowing salinities (the greater of any reach pair) decrease monotonically as one moves up any branch of the estuary, but this is not true of the seaward-flowing values. Beginning at Pillar Point the seaward-flowing salinities (the lesser of any reach pair) first decrease to Point Jefferson, then increase in Colvos Passage before decreasing again up the main axis of the Sound. The Colvos Passage salinity always exceeds that of the neighboring 30-to-50 m deep surface layers because Colvos Passage flows seaward throughout its entire depth range (Figure 8e), and salty water from as deep as 125 m contributes to the flux-weighted salinity there. The lowest salinities in the Sound occur in the shallow, surface layers of fjordlike Hazel Point and Saratoga Passage reaches. The overall means and standard deviations of the flux-weighted salinities for the period 15 February 1953 to 15 March 1955 are tabulated in Table 12.

The flux-weighted salinity time series possess varying degrees of correlation (Table 9). Off Pillar Point, the upper and lower layers correlate well ($r = 0.85$); whereas off New Dungeness the correlation is not significantly different from 0 at the 5% level as indicated by a blank in the table. The lower layer there follows most closely that off Pillar Point ($r = 0.87$), its source of salt water. The upper layer responds much more like the layers along the main axis of Puget Sound ($r \geq 0.87$). All of the main-axis salinities track well (Figure 10b) with $r \geq 0.94$. Layers 13 through 16 are highly correlated ($r \geq 0.85$) within Hood Canal and with the Sound's main

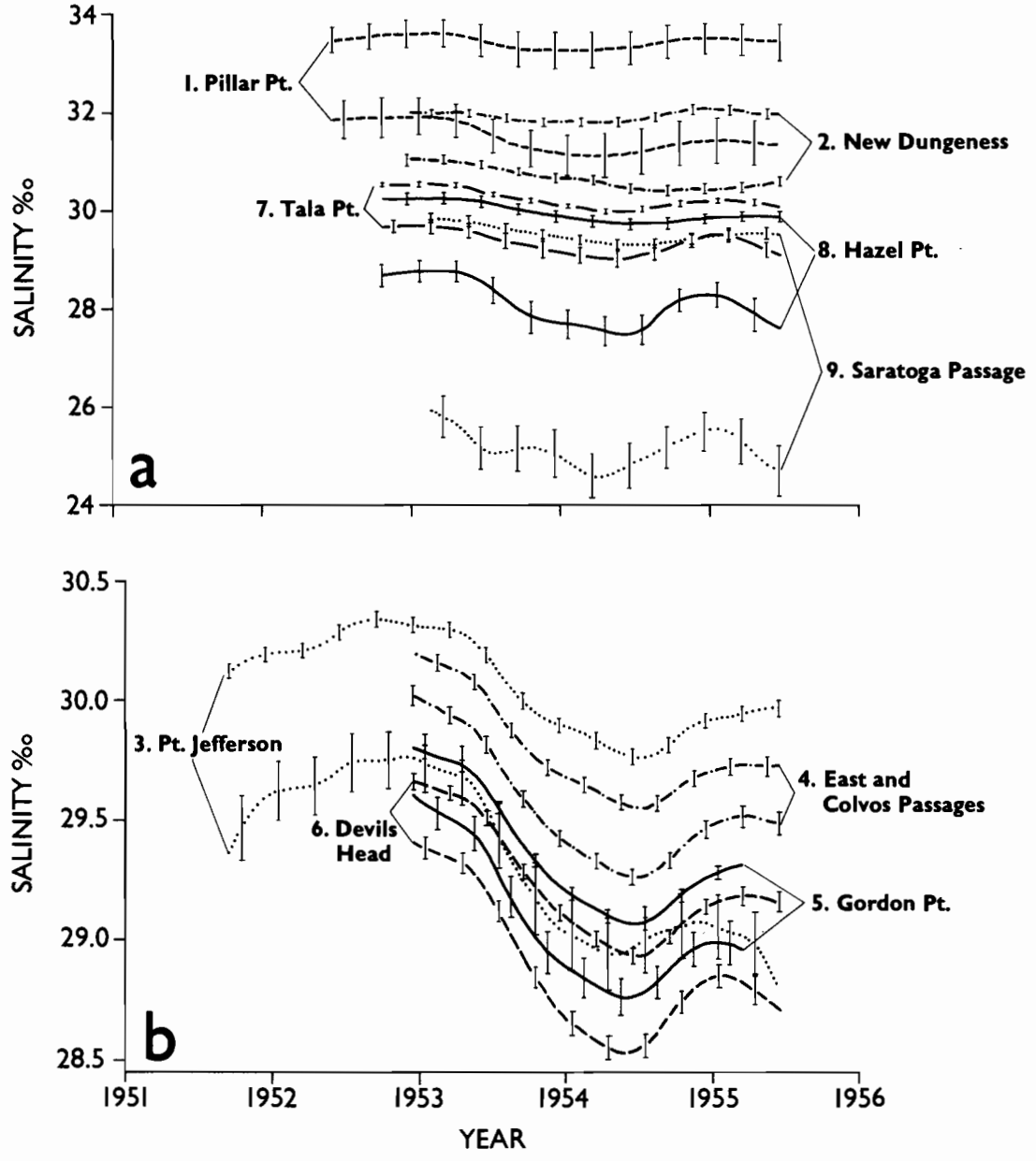

Figure 10. Time series of the annual mean flux-weighted salinity S_i for each reach layer (a) in the Strait of Juan de Fuca, Hood Canal and Saratoga Passage, and (b) along the main axis of Puget Sound. For each pair the landward-flowing salinity always exceeds the seaward-flowing value.

TABLE 9. Correlations between the flux-weighted salinities. Blanks indicate correlations not significantly different from 0 at the 5% level.

	Reach Layer	1	2	3	4	5	6	7	8	9	10	11	12	13	14	15	16	17	18
1	Pillar Pt. lower	1																	
2	Pillar Pt. upper	0.85	1																
3	New Dungeness lower	0.87	0.57	1															
4	New Dungeness upper		0.75		1														
5	Pt. Jefferson lower	0.70	0.96		0.91	1													
6	Pt. Jefferson upper	0.63	0.93		0.90	0.96	1												
7	East Passage	0.65	0.94		0.93	1.00	0.95	1											
8	Colvos Passage	0.67	0.94		0.90	1.00	0.94	1.00	1										
9	Gordon Pt. lower	0.67	0.94		0.91	1.00	0.98	1.00	1.00	1									
10	Gordon Pt. upper	0.71	0.96	0.39	0.90	0.99	0.99	1.00	1.00	1.00	1								
11	Devils Head lower	0.65	0.93		0.91	1.00	0.94	1.00	1.00	1.00	0.99	1							
12	Devils Head upper	0.70	0.96	0.41	0.87	0.98	0.96	0.99	0.99	0.99	1.00	0.99	1						
13	Tala Pt. lower	0.76	0.97	0.44	0.84	0.97	0.96	0.97	0.98	0.98	0.99	0.98	0.99	1					
14	Tala Pt. upper	0.86	0.94	0.67	0.63	0.88	0.85	0.86	0.89	0.89	0.90	0.88	0.92	0.95	1				
15	Hazel Pt. lower	0.62	0.91		0.94	0.99	0.95	0.99	0.99	0.99	0.98	0.99	0.97	0.96	0.85	1			
16	Hazel Pt. upper	0.84	0.95	0.62	0.68	0.89	0.90	0.88	0.89	0.91	0.92	0.89	0.94	0.95	0.98	0.86	1		
17	Saratoga Passage lower	0.55	0.89		0.88	0.99	0.87	0.98	0.99	0.99	0.98	0.99	0.97	0.95	0.83	0.99	0.82	1	
18	Saratoga Passage upper	0.78	0.82	0.67		0.64	0.67	0.65	0.68	0.69	0.71	0.67	0.75	0.82	0.91	0.60	0.87	0.64	1

axis. In Saratoga Passage the lower layer follows that of the main axis ($r \geq 0.87$) while the upper layer responds much like the upper layers in Hood Canal ($r \geq 0.87$).

Some tantalizing correlations exist between the flux-weighted salinities and the runoff (Table 10). The correlations are all negative as to be expected. Fourteen of the eighteen salinities correlate most highly ($|r| \geq 0.89$) with the Skagit River runoff R_9 (included is S_{16} for which $r = -0.89$ is not significantly different from $r = -0.90$ for runoffs R_3 and R_5). This generalizes the results of Ebbesmeyer *et al.* (1989) who found a correlation of –0.81 over 13 years between the Skagit River discharge and the annually averaged salinity at 150 m depth off Point Jefferson and Point No Point a few kilometers to the north. Evidentally the Skagit River water is a tracer with strong potential as a predictor in most of Puget Sound. The lower-layer salinities in the Strait of Juan de Fuca, S_1 and S_3, bear no significant linear relationship (at the 5% level) to the Fraser River runoff, R_1. Their maximum correlations are with small rivers, R_6 and R_8, at the southern end of the Sound. These are probably secondary correlations—the primary ones being with climatic variables not considered here such as the Pacific Ocean salinity.

The salinities of the 1951–1956 period may be representative of the average climatic conditions rather than of just cool, wet years. Ebbesmeyer *et al.* (1989) found no significant correlation between a regional climate index PNW (based on snow depth and water temperature) and the salinity at 150 m off Point Jefferson. Also their analysis showed that annually averaged density profiles for this period, which are closely related to the salinities, bracketed 12 of the 14 available. Therefore the 1950's data set may encompass most of the natural range of salinity variability in Puget Sound.

To shed some light on what factors are responsible for the uncertainty in the flux-weighted salinity we have evaluated the relative contributions of the time-mean salinity and velocity errors to the total variance (15). The two terms contribute in varying degrees (Table 11). At one extreme is Pillar Point reach where velocity fluctuations across the channel account for up to 99% of the variance, and at the other extreme are East and Colvos Passages where fluctuations in the mean salinity contribute most.

7. TRANSPORT

The transport at several sites has been estimated previously by a variety of techniques. Few cover annual periods, and none consider all the reaches. Some estimates have used dissolved oxygen as a nonconservative tracer (Ebbesmeyer and Barnes, 1980; Ebbesmeyer *et al.*, 1984), but these suffer from uncertainties in the oxygen utilization rate. One estimate has come from drift-pole observations in a physical hydraulic model of the Sound, but this is uncertain due to the effects of small scale (Ebbesmeyer and Barnes, 1980). Some estimates have been made from mass conservation applied to runoff and hydrographic records without the benefit of recently available current meter records (Friebertshauser and Duxbury, 1972). Still others have come from current meter records but without regard to mass conservation (Barnes and Ebbesmeyer,

TABLE 10. Correlations between the flux-weighted salinities and the runoff.

	Reach Layer	R_1	R_2	R_3	R_4	R_5	R_6	R_7	R_8	R_9
1	Pillar Pt. lower		–0.70	–0.83	–0.77	–0.82	–0.87	–0.76	–0.75	–0.70
2	Pillar Pt. upper	–0.66	–0.87	–0.92	–0.88	–0.90	–0.82	–0.64	–0.66	–0.95
3	New Dungeness lower		–0.56	–0.72	–0.69	–0.75	–0.87	–0.86	–0.89	–0.46
4	New Dungeness upper	–0.97	–0.51	–0.44	–0.40	–0.38				–0.81
5	Pt. Jefferson lower	–0.82	–0.77	–0.82	–0.79	–0.81	–0.70	–0.57	–0.59	–0.94
6	Pt. Jefferson upper	–0.83	–0.81	–0.85	–0.84	–0.84	–0.72	–0.49	–0.52	–0.92
7	East Passage	–0.83	–0.72	–0.71	–0.66	–0.66	–0.50			–0.95
8	Colvos Passage	–0.81	–0.72	–0.72	–0.67	–0.68	–0.53		–0.37	–0.97
9	Gordon Pt. lower	–0.82	–0.72	–0.72	–0.68	–0.68	–0.53	–0.41	–0.42	–0.97
10	Gordon Pt. upper	–0.80	–0.76	–0.77	–0.73	–0.73	–0.58	–0.45	–0.45	–0.96
11	Devils Head lower	–0.82	–0.70	–0.71	–0.65	–0.66	–0.52			–0.96
12	Devils Head upper	–0.77	–0.76	–0.78	–0.73	–0.74	–0.60		–0.37	–0.96
13	Tala Pt. lower	–0.76	–0.85	–0.85	–0.82	–0.82	–0.69	–0.44	–0.47	–0.97
14	Tala Pt. upper	–0.54	–0.85	–0.90	–0.87	–0.89	–0.83	–0.57	–0.61	–0.92
15	Hazel Pt. lower	–0.87	–0.70	–0.69	–0.65	–0.65	–0.49			–0.94
16	Hazel Pt. upper	–0.59	–0.85	–0.90	–0.88	–0.90	–0.81	–0.49	–0.53	–0.89
17	Saratoga Passage lower	–0.79	–0.56	–0.58	–0.49	–0.52	–0.39			–0.96
18	Saratoga Passage upper		–0.92	–0.90	–0.91	–0.89	–0.82	–0.49	–0.55	–0.79

TABLE 11. Average percentage contribution to the within-year variance $\overline{\Delta S_i^2}$ in the flux-weighted salinities.

Reach	Landward-flowing layer: Due to $\overline{(\Delta\bar{S})^2}^{1/2}$	Due to $\overline{(\Delta\underset{\sim}{\bar{u}}\cdot\underset{\sim}{n})^2}^{1/2}$	Seaward-flowing layer: Due to $\overline{(\Delta\bar{S})^2}^{1/2}$	Due to $\overline{(\Delta\underset{\sim}{\bar{u}}\cdot\underset{\sim}{n})^2}^{1/2}$
1 Pillar Pt.	4	96	1	99
2 New Dungeness	58	42	77	23
3 Pt. Jefferson	75	25	65	35
4 East and Colvos Passages	97	3	99	1
5 Gordon Pt.	85	15	28	72
6 Devils Head	86	14	62	38
7 Tala Pt.	62	38	33	67
8 Hazel Pt.	6	94	19	81
9 Saratoga Passage	16	84	46	54

1978; Cannon and Ebbesmsyer, 1978; Godin, Candela and Paz-Vela, 1981; Cannon, 1983; Ebbesmeyer *et al.*, 1984; Bretschneider *et al.*, 1985; Cannon and Bretschneider, 1986). From these studies it is apparent that the transport differs by two orders of magnitude between the reaches and that some refluxing occurs in the mixing zones.

Given the runoff (Figure 7) and the flux-weighted salinities (Figure 10) we calculate the transports from Knudsen's equations (7). Time series of the annual mean landward transports are shown in Figure 11. The corresponding seaward transports are highly correlated ($r \geq 0.99$) and differ by only the small increment of the runoff. The means and standard deviations for each time series are given in Table 12 for the period 15 Feb 1953 to 15 March 1955. Notice that the transports obtained from substituting the mean cumulative runoff (Table 5) and salinities (Table 12) into Knudsen's equations (7) do not exactly match the transport time series means because Knudsen's equations are nonlinear in the salinities.

TABLE 12. The overall mean flux-weighted salinities and transports with their standard deviations.

	Reach Layer	Salinity ‰	Transport m^3/s
1	Pillar Pt. lower	33.41 ± 0.27	99814 ± 7391
2	Pillar Pt. upper	31.41 ± 0.39	106185 ± 7680
3	New Dungeness lower	31.94 ± 0.13	41166 ± 9553
4	New Dungeness upper	30.68 ± 0.29	42806 ± 9590
5	Pt. Jefferson lower	29.96 ± 0.21	13583 ± 1881
6	Pt. Jefferson upper	29.19 ± 0.38	13941 ± 1861
7	East Passage	29.77 ± 0.27	31632 ± 2085
8	Colvos Passage	29.52 ± 0.31	31891 ± 2047
9	Gordon Pt. lower	29.32 ± 0.32	14421 ± 1893
10	Gordon Pt. upper	29.03 ± 0.36	14565 ± 1895
11	Devils Head lower	29.20 ± 0.31	5143 ± 471
12	Devils Head upper	28.85 ± 0.38	5206 ± 476
13	Tala Pt. lower	30.23 ± 0.25	6617 ± 723
14	Tala Pt. upper	29.34 ± 0.31	6818 ± 717
15	Hazel Pt. lower	29.95 ± 0.24	2521 ± 321
16	Hazel Pt. upper	28.07 ± 0.56	2687 ± 309
17	Saratoga Passage lower	29.53 ± 0.23	3174 ± 279
18	Saratoga Passage upper	25.19 ± 0.62	2595 ± 342

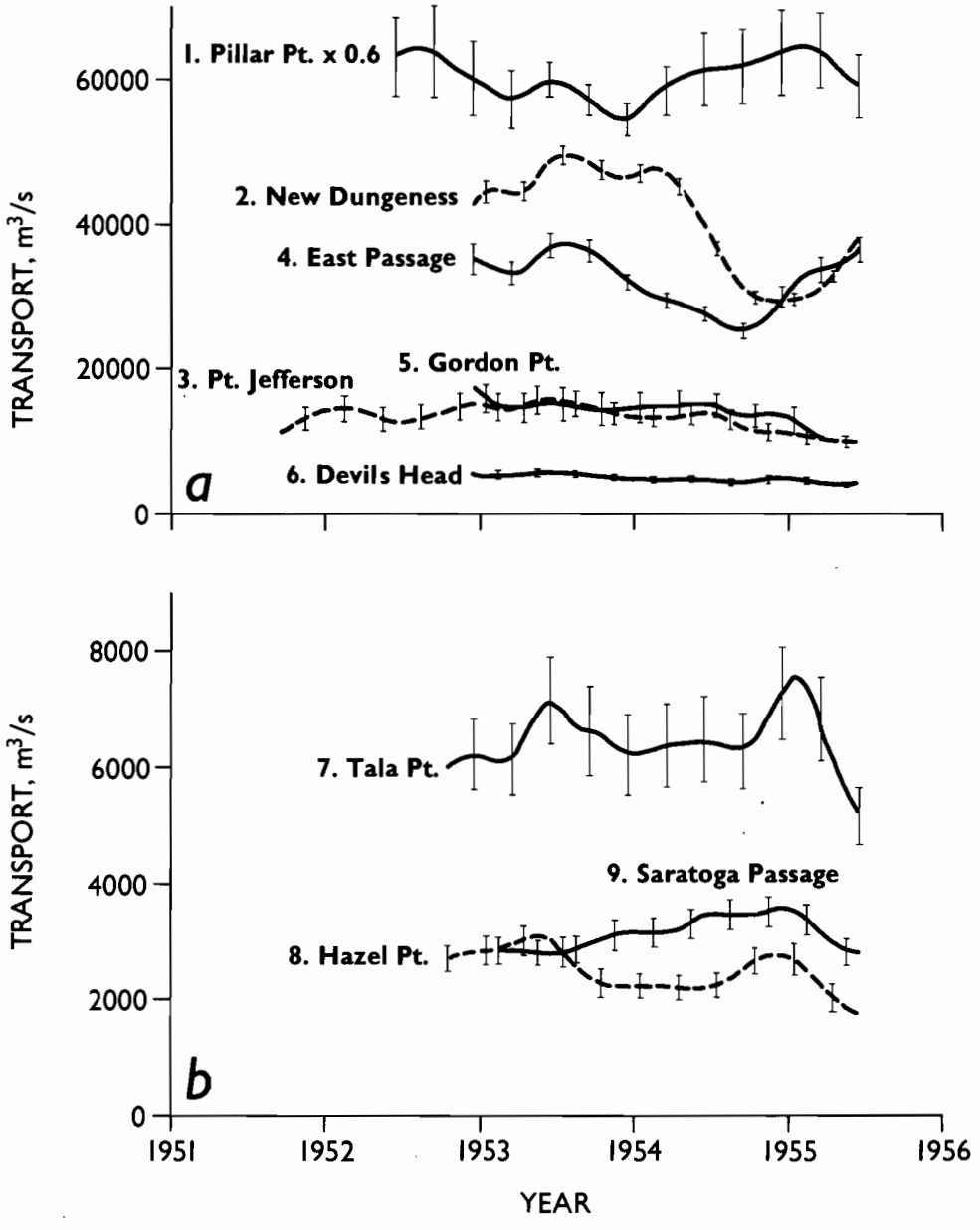

Figure 11. Time series of the annual mean landward transports $Q_{2j-1}/\overline{\rho}$ in each reach of (a) the Strait of Juan de Fuca and along the main axis of Puget Sound, and (b) Hood Canal and Saratoga Passage. The seaward transports differ only by the runoff which is nearly imperceptible at this scale. Note the scaling for Pillar Point reach.

The results will be discussed on a regional basis. For comparison purposes the range of the Knudsen transports is defined to be the minimum landward transport minus its standard error and the maximum seaward transport plus its standard error (Table 13). No annual transports based upon year-long measurements of currents have ever been published; therefore no direct comparison with annual mean Knudsen transports is possible. Perhaps the next best thing is to compare with transports calculated from equation (1) using the composite currents of Section 5 since these are averages over almost all available observations. The tabulated range (Table 13) comes from estimates of the landward and seaward flows which differ in theory by only the runoff, but in practice the difference is often much larger.

7.1. Strait of Juan de Fuca

Off Pillar Point the average transport is around 100,000 m^3/s (Figure 11 and Table 12) which is about 15 times the average cumulative runoff (Table 5). The Knudsen transport range agrees well with that of the composite transports (Table 13). An independent, 101-day set of measurements by Godin *et al.* (1981) using 6 cross-channel current meter moorings in the spring of 1973 compares favorably with our results for 1951–1956 (Table 13). Another set of cross-channel observations by Cannon and Bretschneider (1986) gave 134-day mean transports of 113,000 m^3/s landward and 146,000 m^3/s seaward. These measurements were from three separate 40- to 50-day deployments in the spring and autumn of 1976 and the summer of 1977, and some were used in the composite current profile of Figure 8a. They probably overestimate the annual mean transports due to a summer increase in flow.

The Knudsen and composite transports for New Dungeness reach differ substantially (Table 13). The composites themselves are doubtful since they differ by 22,000 m^3/s which is far greater than the associated runoff (1641 m^3/s). This reach is poorly defined geographically, the cross-channel variability of the currents is unknown, and there are uncertainties concerning the flow of water through Rosario Strait. If it carries substantial Fraser River water southward then the effective runoff for this reach would be higher than calculated, and the Knudsen transport would rise. Conversely, if the longitudinal current decreases toward the channel sides then the transport inferred from the velocity observations would be reduced. For these reasons the transport off New Dungeness is considered speculative.

7.2. Puget Sound's Main Axis

The Knudsen transports off Point Jefferson are only 1/3 to 1/2 those of the composite (Table 13). This is surprising since this reach has the most extensive series of current and salinity measurements (Table 7). Published transports from midchannel observations over one-month periods in the winters of 1972 and 1973 yield 42,000 and 43,000 m^3/s, respectively (Barnes and Ebbesmeyer, 1978; Cannon and Ebbesmeyer, 1978). These are not very different from the composite transports because the composite profiles of Figure 8c include these

TABLE 13. Comparison of the volume transports (m^3/s) range from Knudsen's equations with composite transports and previous estimates.

Reach	Knudsen Transports	Composite Transports	Previous Estimates	Reference	Method
1 Pillar Pt.	87,000–125,000	85,000–97,000	81,000–112,000	Godin *et al.*, 1981	Cross-channel current moorings
			113,000–146,000	Cannon & Bretschneider, 1986	Cross-channel current moorings
2 New Dungeness	28,000–54,000	62,000–84,000	–	–	–
3 Pt. Jefferson	9,000–19,000	25,000–38,000	42,000-43,000	Barnes & Ebbesmeyer, 1978; Cannon & Ebbesmeyer, 1978	Midchannel current mooring
			27,000	Ebbesmeyer & Barnes, 1980	O_2 utilization
			22,000-30,000	Ebbesmeyer & Barnes, 1980	Hydaulic model drifters
			32,000	Ebbesmeyer *et al.*, 1984	0.75 × Cannon & Ebbesmeyer, 1978
			20,000–22,000	Ebbesmeyer *et al.*, 1984	Cross-channel current moorings
4 East Passage	24,000–40,000	32,000	38,000	Cannon, 1983	Midchannel current mooring
			21,000–23,000	Bretschneider *et al.*, 1985	Cross-channel current moorings
Colvos Passage	24,000–40,000	28,000	25,000	Barnes & Ebbesmeyer, 1978	Midchannel current mooring
			27,000	Cannon, 1983	Midchannel current mooring
			26,000	Bretschneider *et al.*, 1985	Midchannel current mooring
5 Gordon Pt.	8,400–21,000	4,000–11,000	–	–	–
6 Devils Head	3,800–6,500	5,200–6,700	–	–	–
7 Tala Pt.	4,500–8,900	6,900–19,000	5,000	Ebbesmeyer *et al.*, 1984	O_2 utilization
8 Hazel Pt.	1,500–3,600	1,500–1,600	1,000–2,000	Ebbesmeyer *et al.*, 1984	O_2 utilization
9 Saratoga Passage	1,900–3,800	1,700–2,300	2,400	Barnes & Ebbesmeyer, 1978	Midchannel current mooring

measurements. From Knudsen's equations (7) an underestimate of the runoff or an overestimate of the lower-to-upper layer salinity difference would reduce the strength of the predicted flows, but it is difficult to believe that either could differ by a sufficient amount, especially considering the long-term annual averaging process. If the associated runoff were too low for this site, one would expect it to be too low elsewhere along the main axis of the Sound, but the observed and predicted flows agree at the other locations. It is unlikely that the surface layer is too fresh at midchannel and hence unrepresentative of the cross-channel mean, especially considering the depth (50 m) of the layer. On the other hand, excessive composite transports could result from an overscaling of the laterally averaged current based solely upon midchannel values. The channel cross section changes drastically near Point Jefferson. At midchannel the mean current bears 46°T (Table 8) which parallels the local bottom topography but resembles little the deeply embayed shoreline. There is other evidence that midchannel currents overestimate the mean transport at this site owing to cross-channel variability. Ebbesmeyer and Barnes (1980) using dissolved oxygen as a tracer deduced mean flows of 27,000 m^3/s. They also observed scaled flows of 22,000–30,000 m^3/s using drifters in the Puget Sound hydraulic model. Subsequently Ebbesmeyer *et al.* (1984) reduced the midchannel transports of Cannon and Ebbesmeyer (1978) to three-quarters of their original value or 32,000 m^3/s (Table 13). Additionally, Ebbesmeyer *et al.* (1984) have assembled a composite cross section in this reach composed of 4 moorings spanning the channel. The records are not concurrent and are of varying lengths but occur between 15 April and 28 September 1976. The observed transport (20,000 to 22,000 m^3/s) is close to the upper limit of the Knudsen range (9,000–19,000 m^3/s).

The transports decrease as one moves landward from the Strait of Juan de Fuca up the main axis of Puget Sound (Figure 11a). However, this pattern is interrupted in East and Colvos Passages where the transport increases before decreasing again off Gordon Point and Devils Head. Substantial clockwise recirculation around Vashon Island is required for the East and Colvos Passage transports to be approximately twice those of the surrounding reaches and for the Colvos Passage salinity to exceed that of the Point Jefferson upper layer (Section 6). This refluxing has been noticed in the Puget Sound hydraulic model (Farmer and Rattray, 1963) but not quantified. It will be considered in future work.

The observed transports in East and Colvos Passages agree rather well with the Knudsen transport range of 24,000–40,000 m^3/s (Table 13). In East Passage the transport has been calculated from an independent midchannel measurement by Cannon (1983) to be 38,000 m^3/s for March 1977. Bretschneider *et al.* (1985) found that midchannel observations gave 33,000 m^3/s in April 1983, but cross-channel arrays of current meters at the same site and nearby reduced this to 21,000 to 23,000 m^3/s. Week- to month-long observations in Colvos Passage (Barnes and Ebbesmeyer, 1978; Cannon, 1983; Bretschneider *et al.*, 1985) gave transports of 25,000 to 27,000 m^3/s.

No transports have been published for Gordon Point reach 5. The composite transports (4,000–11,000 m^3/s) overlap with, but in general are less than, the predicted values (8,400–21,000 m^3/s, Table 13). However the currents there are poorly sampled, especially in the lower layer (Figure 8f).

A somewhat similar situation exists for Devils Head reach 6. The composite current profile is mostly based on 14 days of observations at 3 depths in April 1978. Nevertheless the predictions (3,800–6,500 m^3/s) and observations (5,200–6,700 m^3/s) overlap (Table 13).

7.3. Hood Canal

In Hood Canal, Tala and Hazel Point reach transports differ by a factor of 2 to 3 (Figure 11b and Table 12). Off Tala Point Ebbesmeyer *et al.* (1984) have estimated the transport to be 5000 m^3/s which is within our predicted range of 4,500–8,900 m^3/s (Table 13). The upper and lower layer composite transports are quite disparate with the landward flow (19,000 m^3/s) being three times the seaward flow (6,900 m^3/s), probably because the fitted cubic (Figure 8h) bows landward too far at 50 to 60 m depth where there is no velocity data to constrain it.

For Hazel Point reach 8 the agreement between the various transport estimates is good (Table 13). We predict a range of 1,500–3,600 m^3/s which encompasses the composite transports (1500–1600 m^3/s) although these are based on only one set of observations in February and March 1978. Ebbesmeyer *et al.* (1984) report 1,000–2,000 m^3/s as inferred by Hinchey using dissolved oxygen as a tracer.

7.4. Saratoga Passage and Deception Pass

Owing to the flow through Deception Pass in mixing zone 9 (Figure 1), the transport in Saratoga Passage cannot be determined from Knudsen's equations. In a sense mixing zone 9 is a limiting case of a triple junction mixing zone (section 5 of I) in which one of the reaches is a river, the Skagit. With only two tracers available, water and salt, more information is required to obtain a closed solution. Matters are further complicated by the fact that Deception Pass is very turbulent due to strong tidal currents, and a sharp salinity gradient exists between Rosario Strait and the inner Pass. Therefore it may not be treated as a purely advective reach.

In mixing zone 9 conservation of total and salt mass give

$$\begin{aligned} Q_D &= Q_{17} - Q_{18} + R_9 \\ S_D Q_D - F_D &= S_{17} Q_{17} - S_{18} Q_{18} \end{aligned} \tag{22}$$

where Q_D is the advective mass flux through the Pass, S_D is the flux-weighted salinity, and F_D is the turbulent salt flux which is directed from saltier Rosario Strait into the Pass (Figure 12). Equations (22) are not sufficient to determine the Saratoga Passage flows, Q_{17} and Q_{18}, from their salinities, S_{17} and S_{18}, and the Skagit River runoff R_9 alone. We must rely upon two other pieces of information provided by the measurements of Collias *et al.* (1973). First, based upon temperature and salinity observations, they concluded that no Rosario Strait water enters layer

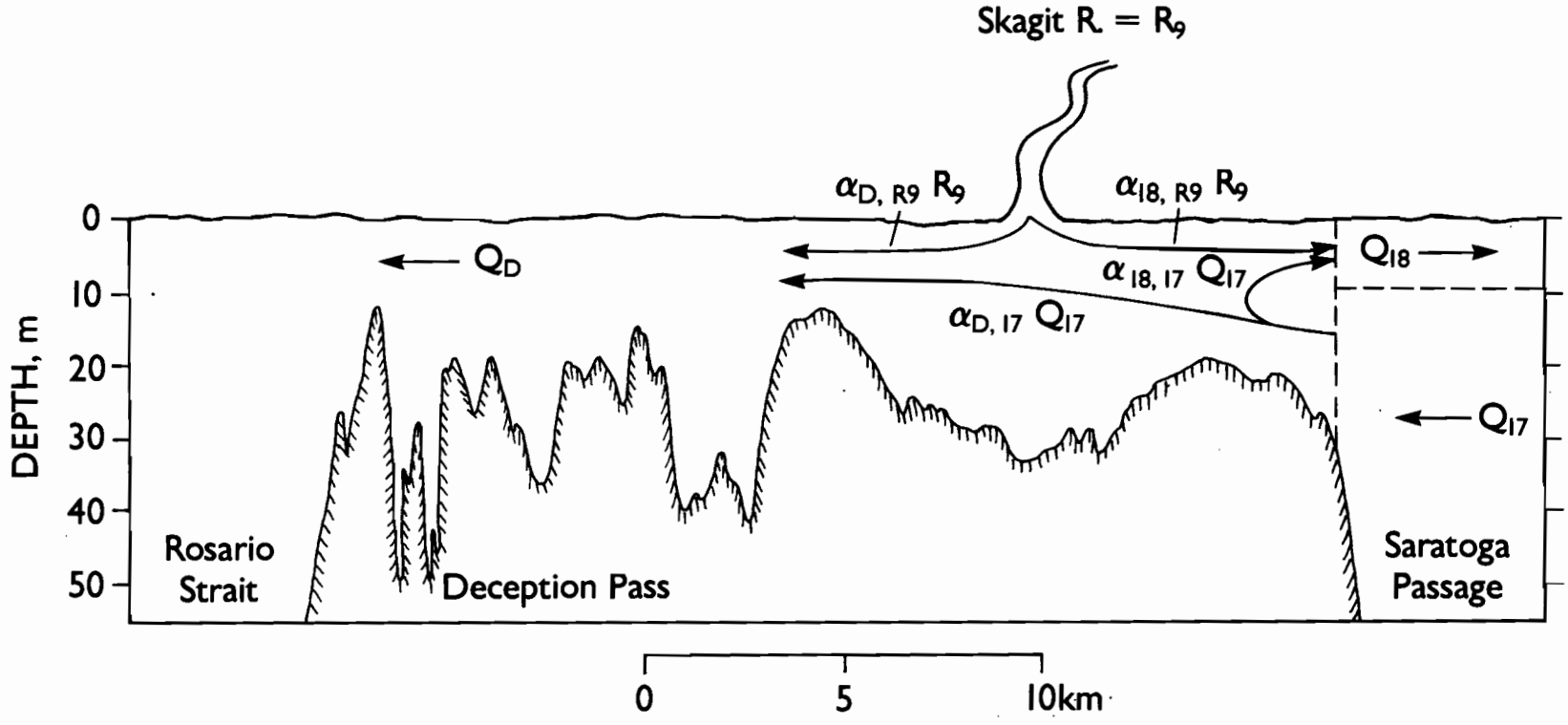

Figure 12. Schematic diagram of the Deception Pass region (adapted from Figure 4-5 of Collias *et al.*, 1973). The mean flow Q_D through Deception Pass is composed of salt water from layer 17 in Saratoga Passage and fresh water from the Skagit River. No water from Rosario Strait enters layer 18 via this pass.

18. This implies that the flows leaving the mixing zone receive water and salt only from layer 17 and the Skagit River, i.e.

$$\begin{aligned} Q_{18} &= \alpha_{18,17}\, Q_{17} + \alpha_{18,R9}\, R_9 \\ S_{18}Q_{18} &= \alpha_{18,17}\, S_{17}\, Q_{17} \\ Q_D &= \alpha_{D,17}\, Q_{17} + \alpha_{D,R9}\, R_9 \\ S_DQ_D - F_D &= \alpha_{D,17}\, S_{17}\, Q_{17} \end{aligned} \tag{23}$$

where α_{ij} is the fraction of layer j water entering layer i (Figure 12). Second, Collias *et al.* (1973) observed that the mean flow in Deception Pass is seaward at about 1125 m^3/s with a standard error of 95 m^3/s. Unfortunately this figure represents the average over only 9 consecutive lunar days in March of 1971, but it is the only such data available. In addition we shall assume that the mixing zone is completely mixed, which is equivalent to

$$\begin{aligned} \alpha_{18,17} &= \alpha_{18,R9} \\ \alpha_{D,17} &= \alpha_{D,R9}\,. \end{aligned} \tag{24}$$

Equations (22) to (24) yield

$$\begin{aligned} Q_{17} &= \frac{S_{18}}{S_{17}-S_{18}} R_9 \\ Q_{18} &= \frac{S_{17}}{S_{17}-S_{18}} R_9 - Q_D \end{aligned} \tag{25}$$

which are similar to Knudsen's equations (7) and

$$\begin{aligned} \alpha_{18,17} &= \alpha_{D,R9} = \frac{S_{17}-S_{18}}{S_{17}} \frac{Q_D}{R_9} \\ \alpha_{D,17} &= \alpha_{18,R9} = 1 - \alpha_{D,R9}\,. \end{aligned} \tag{26}$$

The modified Knudsen equations (25) give lower-layer transports in Saratoga Passage that exceed the upper-layer values (Table 12) because the excess flow leaves mixing zone 9 through Deception Pass. The predicted transport range overlaps the composite transport range and agrees with the previous measurements of Barnes and Ebbesmeyer (1978) based upon a midchannel current meter mooring in July 1970 (Table 13).

Under our assumptions about 66% of the Skagit River flows southward in the surface layer of Saratoga Passage, and the remaining 34% leaves via Deception Pass. Collias *et al.* (1973) independently estimated this partitioning to be 40% and 60%, respectively, by reasoning that all of the Skagit's south-fork flow would enter Saratoga Passage and all of its north-fork flow would leave via Deception Pass with no mixing occurring between the river mouths in the bay. The 40/60 river ratio itself was based on a personal communication with the USGS. If we adopt this assumption, i.e. $\alpha_{18,R9} = 0.4$ and $\alpha_{D,R9} = 0.6$, then $Q_{17}/\overline{\rho} = 2000$ m^3/s, $Q_{18}/\overline{\rho} = 1400$ m^3/s, and $\alpha_{18,17} = 0.6$ as overall average values.

7.5. Comparison with other models

The circulation in Puget Sound has been modeled with conservation of mass techniques in two previous studies. Friebertshauser and Duxbury (1972) divided the Sound into four large basins and computed the transport neglecting turbulent fluxes. They employed an integration of the mass balance equations first applied by Waldichuk (1957) to the Strait of Georgia. In essence these are Knudsen's equations with the addition of terms to account for time variation. A freshwater content of the basin is defined which relies on the implicit assumption that the salinity of the salt water end-member does not vary with time. The source and salinity of this virtual end-member are ambiguous for a sequence of interconnected reaches such as Puget Sound. Analysis of these equations indicates that the salinities therein are actually flux-weighted. Friebertshauser and Duxbury failed to acknowledge this, but even if they had, they lacked sufficient current measurements to perform the flux weighting. They assumed that each upper layer was 10 m deep in rough correspondence to the halocline and averaged over depth to get upper and lower layer salinities. As Table 8 shows, the upper layers are deeper in general. Therefore, we can expect Friebertshauser and Duxbury's salinity contrasts to be too large and their inferred transports to be too small. They did not specify the location or the observation period of their hydrographic stations, but presumably they overlap our own since both of us use the data indexed by Collias (1970) which has the best coverage from 1951 to 1956. Friebertshauser and Duxbury computed runoffs from 1965 to 1968 that are 20% to 80% lower than the 1951–1956 runoffs. They estimated the annual transport for the "entire Puget Sound" (presumed to mean at the northern end of Admiralty Inlet) to be 12,000 to 13,000 m^3/s. This is 1/4 to 1/3 our value for New Dungeness reach. In large part this discrepancy is due to their 3.2‰ lower-to-upper layer salinity difference. We find only about 1.3‰ (Table 12). For southern Puget Sound their transport averaged 3400 m^3/s due to a 1.0‰ salinity difference; whereas at Gordon Point we calculate about 15,000 m^3/s due to a 0.3‰ difference and 37% more runoff. For Tala Point, Friebertshauser and Duxbury calculated a transport of 1500 m^3/s due to a 2.1‰ salinity difference, but our transport is 4 times greater due to 1/2 the salinity difference and twice the runoff. They failed to account for the flow through Deception Pass, hence their annual mean transport in Saratoga Passage (7800–8600 m^3/s) greatly exceeds ours (1900–3800 m^3/s).

Hamilton, Gunn and Cannon (1985) constructed an advective-diffusive box model of the main axis of Puget Sound from Admiralty Inlet to the Narrows. The depth of each upper layer was fixed at 50 m. Unfortunately they did not include the flow in Colvos Passage, but instead relegated this strong seaward flow to an artificial surface layer in East Passage contrary to observation (Figure 8d and e). The upper layer salinities in East Passage were probably not the correct ones to represent this seaward flow. Perhaps because of this, Hamilton *et al.* (1985) found negative eddy diffusivities representing salt diffusion from fresher to saltier water. Their

method of compensating for this counterintuitive behavior is questionable. Nevertheless they computed short-term transports off Point Jefferson of 22,000–27,000 m^3/s for February 1976 based upon a runoff of 538 m^3/s. This is somewhat above our range of annual transports of 9,000–19,000 m^3/s (Table 13) for which the runoff range is 245–411 m^3/s. For East Passage their transports ranged from 17,000 to 19,000 m^3/s over the same time period, but these values are artificial due to their neglect of Colvos Passage. Hamilton *et al.* (1985) also found large transport variations between periods of low runoff in summer and higher runoff in winter. Of particular note is the fact that diffusive fluxes off Point Jefferson were small, and the majority of interlayer exchange occurred in Admiralty Inlet. This is consistent with our partitioning of Puget Sound into horizontal advective reaches separated by mixing zones.

7.6. Knudsen Transport Terms

The terms in Knudsen's equations (7) are coupled, and one cannot reason directly what the response would be to a change in a single term). Table 14 lists the significant correlations (at the 5% level) of each reach's landward transport with the flux-weighted salinities, their difference and the runoff. A first glance at the equations (7) suggests that the landward transport Q_{2j-1} should be negatively correlated with the landward-flowing salinity S_{2j-1} in the denominator. This is true only in New Dungeness and Saratoga Passage reaches; elsewhere the correlations are positive or not significantly different from zero. The explanation of this paradox lies in the balance of the landward and seaward transports; as S_{2j-1} increases so does the seaward transport Q_{2j} and hence the compensating landward transport. The effect of the seaward-flowing salinity S_{2j} on Q_{2j-1} leads to positive correlations everywhere (7). As expected, the surface-to-bottom salinity difference $(S_{2j-1} - S_{2j})$ correlates negatively with the transports, the strongest effects occurring in New Dungeness, East Passage and Hazel Point reaches (Table 14). Perhaps surprisingly the runoff is significantly and positively correlated with the transport in only one reach. Elsewhere the correlations are nullified by the competing effect of the runoff freshening the seaward-flowing layer, thus increasing the salinity difference and decreasing the inferred transport.

7.7. Error Contributions

The within-year transport variance (20) is due to fluctuations in the flux-weighted salinities and the cumulative runoff. The former dominate in the Pillar Point, Point Jefferson, Tala Point and Saratoga Passage reaches (Table 15) where the main contributions come from the upper layer. The flux-weighted salinity errors are due, in turn, to errors in the time-mean salinities and the normal velocities (Table 11). Off New Dungeness and Devils Head the runoff error dominates the transport variance (Table 15).

Throughout this work the slow rate of change of the annually averaged quantities has been neglected. However, Knudsen's equations (7) can be modified to account for this. The largest

TABLE 14. Correlations between the landward transport Q_{2j-1} in each reach and the terms in Knudsen's equations (7).

Reach	Landward-Flowing Salinity S_{2j-1}	Seaward-Flowing Salinity S_{2j}	Salinity Difference $S_{2j-1}-S_{2j}$	Runoff $R_{j\Sigma}$
1 Pillar Pt.	0.48			
2 New Dungeness	–0.71	0.71	–0.91	
3 Pt. Jefferson	0.44	0.58	–0.70	
4 East Passage	0.66	0.69	–0.76	
5 Gordon Pt.			–0.51	
6 Devils Head	0.74	0.74	–0.59	
7 Tala Pt.			–0.62	
8 Hazel Pt.	0.68	0.89	–0.90	
9 Saratoga Passage	–0.86			0.73

TABLE 15. Average percentage contribution to the within-year variance in the transports.

Reach	Due to $\overline{\Delta S_i^2}^{1/2}$	Due to $\overline{\Delta R^2_{j\Sigma}}^{1/2}$
1 Pillar Pt.	86	14
2 New Dungeness	15	85
3 Pt. Jefferson	93	7
4 East and Colvos Passages	47	53
5 Gordon Pt.	89	11
6 Devils Head	10	90
7 Tala Pt.	74	26
8 Hazel Pt.	52	48
9 Saratoga Passage	73	27

contribution comes from the changing salt content landward of any reach. An estimate of these terms shows that they modify the transports by less than 10% with the possible exception of Point Jefferson reach where the modification approaches 20% at times. This source of error is generally within the error bars of Figure 11, but it has not been included explicitly. This supports our assumption that the time series of mean annual transports varies slowly enough that it can be constructed from a sequence of steady approximations.

8. SUMMARY AND CONCLUSIONS

The Strait of Juan de Fuca and Puget Sound have been partitioned into a series of 9 advective reaches separated by mixing zones where turbulent transport may dominate. We have refined a technique (Lincoln, 1977) for computing the runoff into the estuary. Composite velocity profiles of long-term mean currents have been generated from sporadic, modern observations and have been coupled with periodically sampled, historical salinity measurements to calculate the flux-weighted salinity in a two-layered model.

Fresh water and salt are two tracers sufficient to apply conservation of mass techniques to deduce the annual mean volume transport in the 18 reach layers over a four year period. In the Strait of Juan de Fuca the annual transport averages about 100,000 m^3/s (Table 12 and Figure 11) in each layer off Pillar Point, and it decreases to about 40,000 m^3/s at the entrance to Puget Sound off New Dungeness. The transports are small (<7,000 m^3/s) and steadily decrease up the Hood Canal and Saratoga Passage side channels of Puget Sound. However, up the main axis the transport decreases to about 14,000 m^3/s (Table 12) off Point Jefferson but then rises to 32,000 m^3/s in East and Colvos Passages before decreasing again to 15,000 m^3/s off Gordon Point and to 5000 m^3/s off Devils Head. Comparisons with transports inferred from current moorings and oxygen utilization techniques are reasonably good considering the disparity of the techniques and the interannual variability. An error analysis gives estimates of the magnitudes and origins of uncertainties in the transports.

More long-term current meter measurements are required in the estuary. The transports in 3 of the reaches – New Dungeness, Gordon Point, and Devils Head – have never before been calculated, and in 2 more – Tala Point and Hazel – only indirect oxygen utilization methods have been used. These measurements should be combined with moored salinity observations over at least one year to improve our understanding of the mean circulation and its fluctuations.

Based upon available salinity and current observations and simplifying assumptions we have developed a model of the mean flow through Deception Pass. About 1/3 of the strong Skagit River runoff can bypass Puget Sound and flow directly into Rosario Strait. This reduces the transport in Saratoga Passage as inferred by a previous mass conservation estimate in which the leak through Deception Pass was ignored.

A significant amount of recirculation must occur around Vashon Island because the transports in East and Colvos Passages are approximately twice those of the surrounding reaches.

Since the recirculation connects two large cities, Seattle and Tacoma, this could lead to the build-up of contaminants in the southern Sound.

The analyzed runoff and salinity data sets and the inferred transports of the present work provide a foundation for applying the reflux theory (I) to Puget Sound. Even though the physical oceanography of Puget Sound has been studied for the past 60 years no model exists that utilizes this information to predict contaminant concentrations and time scales. These will be the topics of future papers.

9. ACKNOWLEDGMENTS

This paper is dedicated to Clifford A. Barnes and Eugene E. Collias without whose hydrographic sampling program, begun over 35 years ago, our work would not have been possible. We thank the many individuals responsible for the current meter measurements, and we acknowledge the encouragement and support of Herbert C. Curl. We thank Ryan Whitney for manuscript preparation and Gini Curl and Joy Register for graphics. This work was supported in part by the Ocean Assessment Division of the National Ocean Service, National Oceanic and Atmospheric Administration, U.S. Department of Commerce. Contribution 1201 from NOAA's Pacific Marine Environmental Laboratory.

10. REFERENCES

Anderson, T. W. (1971): *The Statistical Analysis of Time Series*, John Wiley & Sons, N.Y., 704 pp.

Barnes, C. A. and E. E. Collias (1954a): Physical and chemical data for Puget Sound and approaches, March-August 1952, *Tech. Rep. No. 24*, University of Washington, Department of Oceanography, 42 pp.

Barnes, C. A. and E. E. Collias (1954b): Physical and chemical data for Puget Sound and approaches, February 1949 - February 1952, *Tech. Rep. No. 28*, University of Washington, Department of Oceanography, 46 pp.

Barnes, C. A. and E.E. Collias (1954c): Physical and chemical data for Puget Sound and approaches, October - December 1952, *Tech. Rep. No. 35*, University of Washington, Department of Oceanography, 61 pp.

Barnes, C.A. and E.E. Collias (1956a): Physical and chemical data for Puget Sound and approaches, January - December 1953. *Tech. Rep. No. 45*, University of Washington, Department of Oceanography, 212 pp..

Barnes, C.A. and E.E. Collias (1956b): Physical and chemical data for Puget Sound and approaches, January 1955 - March 1956. *Tech. Rep. No. 46*, University of Washington, Department of Oceanography, 259 pp.

Barnes, C.A. and E.E. Collias (1956c): Physical and chemical data for Puget Sound and approaches, January 1955 - March 1956. *Tech. Rep. No. 51*, University of Washington, Department of Oceanography, 141 pp.

Barnes, C.A. and C.C. Ebbesmeyer (1978): Some aspects of Puget Sound's circulation and water properties, in *Estuarine Transport Processes*, edited by B. Kjerfve, Univ. South Carolina Press, Columbia, SC, 209–227.

Bretschneider, D.E., G.A. Cannon (1985): J.R. Holbrook, and D.J. Pashinski, Variability of subtidal current structure in a fjord estuary: Puget Sound, Washington. *J. Geophys. Res., 90*, 11949-11958.

Brownlee, K.A. (1984): *Statistical Theory and Methodology in Science and Engineering*, Krieger Publishing Co., Malabar, Florida, 590 pp.

Burns, R. (1985): *The Shape & Form of Puget Sound*, Puget Sound Books, Washington Sea Grant Publication, 100 pp.

Canada, Water Resources Division (1955): Surface water supply of Canada, Pacific Drainage, British Columbia and Yukon Territory: Climatic years 1950-51 and 1951-52, *Water Resources Paper No. 114*, Department of Northern Affairs and National Resources, Ottawa.

Canada, Water Resources Division (1957): Surface water supply of Canada, Pacific Drainage, British Columbia and Yukon Territory: Climatic years 1952-53 and 1953-54, *Water Resources Paper No. 118*, Department of Northern Affairs and National Resources, Ottawa, 449 pp.

Canada, Water Resources Division (1959): Surface water supply of Canada, Pacific Drainage, British Columbia and Yukon Territory: Climatic years 1954-55 and 1955-56, *Water Resources Paper No. 122*, Department of Northern Affairs and National Resources, Ottawa, 650 pp.

Cannon, G.A. (1983): An overview of circulation in the Puget Sound estuarine system. *NOAA Tech. Memo. ERL PMEL-48*, 30 pp.

Cannon, G.A. and D.E. Bretschneider (1986): Interchanges between coastal and fjord circulation. *Rapp. P.-v. Réun. Cons. Int. Explor. Mer., 186*, 38-48.

Cannon, G.A. and C.C. Ebbesmeyer (1978): Winter replacement of bottom water in Puget Sound, in *Estuarine Transport Processes*, edited by B. Kjerfve, Univ. South Carolina Press, Columbia, SC, 229–238.

Cannon, G.A., and J.R. Holbrook (1981): Wind-induced seasonal interactions between coastal and fjord circulations, in *The Norwegian Coastal Current*, edited by R. Saetre and M. Mork, Univ. of Bergen, Norway, 131–151.

Cokelet, E.D., and R.J. Stewart (1985): The exchange of water in fjords: The efflux/reflux theory of advective reaches separated by mixing zones, *J. Geophys. Res., 90*, 7287-7306.

Collias, E.E. (1970): Index to physical and chemical oceanographic data of Puget Sound and its approaches 1932-1966, *Spec. Rep. No. 43, WSG 70-4*, University of Washington, Department of Oceanography.

Collias, E.E., and S.I. Andreeva (1977): *Puget Sound Marine Environment: An annotated bibliography*. Washington Sea Grant Publication, University of Washington Press, Seattle, 392 pp.

Collias, E.E., C.A. Barnes, and J.H. Lincoln (1973): Skagit Bay study dynamical oceanography, final report, *M73-73*, University of Washington, Department of Oceanography, 197 pp.

Collias, E.E., N. McGary, and C.A. Barnes (1974): *Atlas of Physical and Chemical Properties of Puget Sound and its Surrounding Approaches*, University of Washington, Department of Oceanography, 235 pp.

Cox, J.M., C.C. Ebbesmeyer, C.A. Coomes, J.M. Helseth, L.R. Hinchey, G.A. Cannon and C.A. Barnes (1984): Synthesis of current measurements of Puget Sound, Washington - Volume I: Index of current measurements made in Puget Sound from 1908 - 1980 with daily and record averages for selected measurements. *NOAA Tech. Memo. NOS OMS 3.*

Dyer, K.R. (1973): *Estuaries: A Physical Introduction*, John Wiley & Sons, London, 140 pp.

Ebbesmeyer, C.C. and C.A. Barnes (1980): Control of a fjord basin's dynamics by tidal mixing in embracing sill zones, *Estuarine and Coastal Marine Science, 11*, 311-330.

Ebbesmeyer, C.C., C.A. Coomes, G.A. Cannon, and D.E. Bretschneider (1989): Linkage of ocean and fjord dynamics at decadal period, in *Aspects of climate variability in the eastern Pacific and western Americas*, edited by D.H. Peterson and D.G. Aubrey, American Geophysical Union, Washington, DC.

Ebbesmeyer, C.C., C.A. Coomes, J.M. Cox, J.M. Helseth, L.R. Hinchey, G.A. Cannon and C.A. Barnes (1984): Synthesis of current measurements in Puget Sound, Washington - Volume 3: Circulation in Puget Sound: An interpretation based on historical records of currents. *NOAA Tech. Memo. NOS OMS 5.*

Farmer, H.G. and M. Rattray, Jr. (1963): A model study of the steady-state salinity distribution in Puget Sound. *Tech. Rep. No. 85*, University of Washington, Department of Oceanography., 33 pp.

Friebertshauser, M.A., and A.C. Duxbury (1972): A water budget study of Puget Sound and its subregions, *Limnology and Oceanography, 17*, 237-247.

Gill, A. E. (1982): *Atmosphere-Ocean Dynamics*, Academic Press, New York, 662 pp.

Gladwell, J.S. and A.C. Mueller (1967): *An initial study of the water resources of the State of Washington, Vol. II, Parts A & B, Water Resources Atlas of the State of Washington*, The State of Washington Water Research Center, Washington State University, Pullman, WA.

Godin, G., J. Candela and R. Paz-Vela (1981): On the feasibility of detecting net transports in and out of Georgia Strait with an array of moored current meters, *Atmosphere-Ocean, 19*, 148-157.

Hamilton, P., J.T. Gunn and G.A. Cannon (1985): A box model of Puget Sound, *Estuarine, Coastal and Shelf Science, 20*, 673-692.

Hansen, D.V. and M. Rattray, Jr. (1965): Gravitational circulation in straits and estuaries, *J. Mar. Res. 23*, 104-122.

Hansen, D. V., and M. Rattray, Jr. (1966): New dimensions in estuary classification, *Limnol. Oceanogr., 11*, 319–326.

Holbrook, J.R., G.A. Cannon, and D.G. Kachel (1983): Two-year observations of coastal-fjord interactions in the Strait of Juan de Fuca, in *Coastal Oceanography*, edited by H. Gade, A. Edwards and H. Svendsen, Plenum Press, NY, 411–426.

Holbrook, J.R., R.D. Muench, D.G. Kachel, and C. Wright (1980): Circulation in the Strait of Juan de Fuca: Recent oceanographic observations in the Eastern Basin, *NOAA Tech. Rep. ERL 412 - PMEL 33*, 42 pp.

Joint Committee on Oceanography (1955): Physical and chemical data record, Juan de Fuca Strait project, 1951-52. *File N 6-24(1)*, Pacific Oceanographic Group, Nanaimo, British Columbia.

Knudsen, Martin (1900): Ein hydrographischer Lehrsatz. *Ann. d. Hydr. U. Marit. Meteorol., Vol. 28*, 316-320 (English translation by C.D. Mobley, NOAA/NESDIS Library, Seattle, WA, 1983).

Laird, N.P. and J.A. Galt (1975): Observations of currents and water properties in Puget Sound, 1973, *NOAA Tech. Rep. ERL 327 - PMEL 23*, 141 pp.

Larsen, J.C. (1980): Electromagnetic response functions from interrupted and noisy data, *J. Geophys. Geoelectr., 32*, SI89-SI103.

Larsen, L.H., N. Shi and J.G. Dworski (1977): Current meter observations in Colvos Passage: Puget Sound, March 1977, *Special Report No. 82*, M77-117, University of Washington, Department of Oceanography.

Lincoln, J.H. (1977): Derivation of freshwater inflow into Puget Sound, *Special Rep. No. 72*, University of Washington, Department of Oceanography.

Officer, C.B. (1977): Longitudinal circulation and mixing relations in estuaries, in *Estuaries, Geophysics and the Environment*, National Academy of Sciences, Washington, DC, 13–21.

Okubo, A. (1971): Oceanic diffusion diagrams, *Deep Sea Res., 18*, 789–802.

Proehl, J.A. & M. Rattray, Jr. (1984): Low frequency response of wide deep estuaries to non-local atmospheric forcing, *J. Phys. Ocean., 14*, 904-921.

Shoemaker, D.P., C.W. Garland & J.I. Steinfeld (1974): *Experiments in Physical Chemistry*, 3rd Edition, McGraw-Hill, N.Y.

Snedecor, G.W. and W.G. Cochran (1980): *Statistical Methods.* Seventh edition, Iowa State University Press, Ames, Iowa, 507 pp.

Thomson, R.E. (1981): *Oceanography of the British Columbia Coast*, Canadian Special Publication of Fisheries and Aquatic Sciences 56, Ottawa, 291 pp.

United States Coast and Geodetic Survey (1989): *Pacific Coast. Coast Pilot of California, Oregon and Washington*, Washington, D.C.

United States Geological Survey (1964): Compilation of records of surface waters of the United States. October 1950 to September 1960. Part 12. Pacific slope basins in Washington and Upper Columbia River Basin. *Geological Survey Water-Supply Paper 1736.* U.S. Government Printing Office.

University of Washington, Department of Oceanography (1953): *Puget Sound and approaches. A literature survey*, Volume I: Geography, climatology, hydrology, Seattle.

Waldichuk, M. (1957): Physical oceanography of the Strait of Georgia, British Columbia. *J. Fish. Res. Bd. Canada 14*, 321-486.

Washington Office of Financial Management (1987): 1987 Populations Trends for Washington State, Rep. F87-08, Olympia, 57 pp.

11. APPENDIX

The moving average of a time series is a low pass filter. The output from such a filter may be used in a consistent fashion with the time-averaged equations derived in I. The integral in (13) can be computed even for unequally spaced data by interpolating the integrand to the limits of integration using a polynomial consistent with the quadrature rule. No moving averages are available for a period equal to one-half the averaging interval at the beginning and end of the record. The method of calculating the twelve-month moving average and estimating its uncertainty from data which contain a strong seasonal signal plus noise is outlined in Section 2. The details are presented below.

To estimate the signal we smooth the time series with a moving average. An arbitrary time varying function f(t) may be written as:

$$f(t) = \phi(t) + \varepsilon(t). \tag{A.1}$$

where $\phi(t)$ is the signal and $\varepsilon(t)$ is the noise. Suppose we measure f(t) at discrete, equally spaced instances of time t_i denoted by a subscript. Then we may estimate the signal by a moving average (Anderson, section 3.3, 1971) denoted by an asterisk and defined by

$$\begin{aligned} f_i^* &= \sum_{j=-m}^{m} c_j f_{i+j} \\ &= \sum c_j \phi_{i+j} + \sum c_j \varepsilon_{i+j} \\ &= \phi_i^* + \varepsilon_i^* \end{aligned} \tag{A.2}$$

where the weighting factors c_j and the summation limits m depend upon the form of the moving average chosen which is usually some low-order polynomial. We assume that the noise is random; it has zero mean, a constant variance σ^2 and is uncorrelated, i.e.

$$\begin{aligned} &E\ \varepsilon_i = 0 \\ &\text{Var}\ \varepsilon_i = \sigma^2 \\ &E\ \varepsilon_i \varepsilon_j = 0 \end{aligned} \tag{A.3}$$

where E represents the expected value operator and Var the variance operator. From equations (A.1) and (A.3) the observed time series has an expected value given by

$$\begin{aligned} E\ f_i &= E\ \phi_i + E\ \varepsilon_i \\ &= \phi_i \end{aligned} \tag{A.4}$$

and a variance given by

$$\begin{aligned} \text{Var}\ f_i &= E(f_i - \phi_i)^2 \\ &= \sigma^2 . \end{aligned} \tag{A.5}$$

Likewise from equations (A.1) to (A.4) the moving averaged time series has a mean given by

$$\begin{aligned} E\, f_i^* &= E \sum_{j=-m}^{m} c_j f_{i+j} \\ &= \sum_{j=-m}^{m} c_j \phi_{i+j} \end{aligned} \tag{A.6}$$

and a variance given by

$$\begin{aligned} \text{Var}\, f_i^* &= E\left(f_i^* - E\, f_i^*\right)^2 \\ &= E\left[\sum_{j=-m}^{m} c_j\left(f_{i+j} - \phi_{i+j}\right)\right]^2 \\ &= E\left(\sum_{j=-m}^{m} c_j\, \varepsilon_{i+j}\right)^2 \\ &= \sigma^2 \sum_{j=-m}^{m} c_j^2 \,. \end{aligned} \tag{A.7}$$

In the averaging process the $|c_j|$'s are less than unity; therefore the variance (A.7) of the moving average is less than that (A.5) of the original time series.

The purpose of smoothing is to estimate the signal with reduced error. The error comes from a systematic bias and from a random part which is measured by the variance (A.7) (Anderson, section 3.3, 1971). The former is due to the fact that the expected value of the observed time series does not equal that of the smoothed time series, i.e. from (A.4) and (A.6)

$$\begin{aligned} E\left(f_i - f_i^*\right) &= \phi_i - \sum_{j=-m}^{m} c_j\, \phi_{i+j} \\ &\neq 0 \end{aligned} \tag{A.8}$$

in general. This is the tendency of a moving average to round off highs and lows of the signal itself unless the degree of the moving average polynomial is greater than or equal to that of the underlying signal. We estimate the magnitude of the bias by the arithmetic mean of the residuals $f_i - f_i^*$ over the entire time series. The factor σ^2 in (A.7) is unknown, but it can be related to the variance of the residuals by

$$\begin{aligned} \text{Var}(f_i - f_i^*) &= E\,[(f_i - f_i^*) - E(f_i - f_i^*)]^2 \\ &= E\,[(f_i - E\, f_i) - (f_i^* - E\, f_i^*)]^2 \\ &= E\,(\varepsilon_i - \varepsilon_i^*)^2 \\ &= E\,(\varepsilon_i^2 - 2\varepsilon_i\varepsilon_i^* + \varepsilon_i^{*2}) \end{aligned}$$

$$= \left(1 - 2c_o + \sum_{j=-m}^{m} c_j^2\right) \sigma^2 \ . \qquad \text{(A.9)}$$

Therefore from (A.7) and (A.9) we have

$$\text{Var } f_i^* = \frac{\sum_{j=-m}^{m} c_j^2}{1 - 2\,c_o + \sum_{j=-m}^{m} c_j^2} \text{ Var } \left(f_i - f_i^*\right) \qquad \text{(A.10)}$$

where Var $(f_i - f_i^*)$ is computed in the usual manner. In summary, the squared error in the moving average is the sum of (A.10) and the square of (A.8).

We adopt for our moving average an arithmetic mean centered on 2m+1 points which is nearly equivalent to integrating equation (4) via the trapezoidal rule. The coefficients c_j are given by

$$c_j = \frac{1}{2m+1} \ , \qquad j = 0, \pm 1, ..., \pm m, \qquad \text{(A.11)}$$

In this case (A.10) reduces to

$$\text{Var } f_i^* = \frac{\text{Var}\left(f_i - f_i^*\right)}{2m} \ . \qquad \text{(A.12)}$$

The signal is approximated by a three-month moving average since the length of one season is a natural time scale. For data tabulated monthly m = 1, and (A.11) becomes $c_j = 1/3$. Therefore from (A.7) the variance of the moving average is 1/3 that of the observations. The bias incurred (A.8) is generally small, equalling about 9% for a sinusoidal annual signal (Anderson, section 3.3, Eq. (34), 1971).

The formulae derived so far depend upon the data being tabulated at equispaced time intervals. Any attempt at carrying out the derivation for unequal spacing is futile since the coefficients c in (A.2) depend upon both i and j. In that case the data are interpolated to equally spaced intervals using piecewise continuous first order polynomials, and then the techniques described above are applied. However in order to compensate partially for the unequal data spacing, the estimate of the variance of the signal (A.12) is modified to

$$\text{Var } f_i^* \approx \frac{\text{Var}\left(f_i - f_i^*\right)}{N_i - 1} \qquad \text{(A.13)}$$

where N_i is the total number of original data points actually employed in the calculation of each f_i^*. For example, whenever the original data spacing exceeds the length of the moving average $N_i = 2$ since then only two of the original data values are being employed to calculate the average.

To evaluate the centered twelve-month moving average, denoted by an overbar, we compute the arithmetic mean of the three-month averages which are tabulated monthly. The formula is

$$\begin{aligned} \bar{f}_i &= \sum_{j=-6}^{6} a_j f^*_{i+j} \\ a_j &= 1/12, \qquad j = 0, \pm1,...,\pm5, \\ a_{\pm6} &= 1/24. \end{aligned} \tag{A.14}$$

which is a discrete approximation to (4).

The uncertainty in $\bar{f}_i$ is approximated by the perturbation method or the method of propagation of errors (Shoemaker, Garland and Steinfeld, 1974). Briefly, if g(x,y,...) is a function of several variables, each of which is known to within some error (x + Δx, y + Δy,...), then these errors propagate to cause an uncertainty Δg in g given by

$$\Delta g \approx \frac{\partial g}{\partial x}\,\Delta x + \frac{\partial g}{\partial y}\,\Delta y + ... \tag{A.15}$$

where higher order terms are neglected. If the errors are random (zero mean and uncorrelated) then

$$\begin{aligned} E\,(g + \Delta g) &\approx E\,(g) \\ \mathrm{Var}\,(g + \Delta g) &\approx \left(\frac{\partial g}{\partial x}\right)^2 E(\Delta x)^2 + \left(\frac{\partial g}{\partial y}\right)^2 E(\Delta y)^2 + ,... \end{aligned} \tag{A.16}$$

An application of the propagation of errors (A.15) to the twelve-month averaging function (A.14) yields

$$\begin{aligned} \Delta\bar{f}_i &\approx \sum_{m=-6}^{6} a_j\left(\Delta f^*_{i+j}\right) \\ &\approx \left(\frac{2}{24^2} + \frac{11}{12^2}\right)\Delta f_i^* \\ &\approx 0.080\ \Delta f_i^*. \end{aligned} \tag{A.17}$$

If for the purpose of illustration (but not in the numerical results of the paper) we neglect the bias (A.8) which contributes to Δf_i^*, then by (A.16), (A.17), (A.7), and (A.11)

$$\mathrm{Var}\ \bar{f}_i \approx 0.027\ \sigma^2. \tag{A.18}$$

This is considerably smaller than the variance $s^2/12 = 0.083\ s^2$ we would have calculated if we had proceeded as suggested initially in Section 3 and simply computed the twelve-month moving average of the observed data. In that case, s^2 exceeds σ^2 since it includes both the short period

(less than 3 months) noise and the variance of the seasonally dominated signal about the twelve-month mean.

☆ U.S. GOVERNMENT PRINTING OFFICE: 1990—773-002/11064

Errata for "The annual mean transport in Puget Sound,"
NOAA Tech. Memo ERL PMEL-92, July 1990

by

E.D. Cokelet, R.J. Stewart, and C.C. Ebbesmeyer

Page	Change
45	Equation (26), $\alpha_{18,17}$ should read $\alpha_{D,17}$ and $\alpha_{D,17}$ should read $\alpha_{18,17}$.
47	Section 7.6, first sentence. Delete the right parenthesis at the end of the sentence.
54	First reference. Date should be 1889, not 1989.